Title

FXR Regulates Intestinal Cancer Stem Cell Proliferation

Journal

Cell, 176(5)

ISSN

0092-8674

Authors

Fu, Ting
Coulter, Sally
Yoshihara, Eiji
et al.

Publication Date

2019-02-01

DOI

10.1016/j.cell.2019.01.036

Peer reviewed

HHS Public Access

Author manuscript

Cell. Author manuscript; available in PMC 2020 February 21.

Published in final edited form as:

Cell. 2019 February 21; 176(5): 1098–1112.e18. doi:10.1016/j.cell.2019.01.036.

FXR regulates intestinal cancer stem cell proliferation

Ting Fu[1], **Sally Coulter**[2], **Eiji Yoshihara**[1], **Tae Gyu Oh**[1], **Sungsoon Fang**[1], **Fritz Cayabyab**[1], **Qiyun Zhu**[3], **Tong Zhang**[4], **Mathias Leblanc**[1], **Sihao Liu**[1], **Mingxiao He**[1], **Wanda Waizenegger**[1], **Emanuel Gasser**[1], **Bernd Schnabl**[5], **Annette R Atkins**[1], **Ruth T Yu**[1], **Rob Knight**[3,6], **Christopher Liddle**[2], **Michael Downes**[1,†], **Ronald M Evans**[1,7,†]

[1]Gene Expression Laboratory, Salk Institute for Biological Studies, La Jolla, CA, 92037

[2]Storr Liver Centre, Westmead Institute for Medical Research and Sydney Medical School, University of Sydney, Westmead, New South Wales, 2145, Australia

[3]Department of Medicine, University of California San Diego, La Jolla, CA, 92037

[4]Waitt Biophotonics Core, Salk Institute for Biological Studies, La Jolla, CA, 92037

[5]Department of Pediatrics, University of California San Diego, La Jolla, CA, 92037

[6]Department of Computer Science and Engineering, University of California San Diego, La Jolla, CA 92037

[7]Howard Hughes Medical Institute, The Salk Institute for Biological Studies, La Jolla, CA 92037

SUMMARY

Increased levels of intestinal bile acids (BAs) are a risk factor for colorectal cancer (CRC). Here we show that the convergence of dietary factors (high-fat diet) and dysregulated WNT signaling (APC mutation) alters BA profiles to drive malignant transformations in Lgr5-expressing ($Lgr5^+$) cancer stem cells and promote an adenoma-to-adenocarcinoma progression. Mechanistically, we show that BAs that antagonize intestinal Farnesoid X receptor (FXR) function, including tauro-β-muricholic acid (T-βMCA) and deoxycholic acid (DCA), induce proliferation and DNA damage in $Lgr5^+$ cells. Conversely, selective activation of intestinal FXR can restrict abnormal $Lgr5^+$ cell

†**Corresponding authors:** Michael Downes and Ronald M. Evans (Lead Contact), Gene Expression Laboratory, The Salk Institute for Biological Studies, 10010 North Torrey Pines Road, La Jolla, CA 92037, downes@salk.edu, evans@salk.edu.

AUTHOR CONTRIBUTIONS

T.F., A.R.A., R.T.Y., M.D. and R.M.E. designed and supervised the research. T.F. performed experiments and analyzed results, with technical assistance from F.C., W.W., and M.H. S.C. and C.L. performed bile acid analyses, T.G.O., C.L. and R.T.Y. analyzed genomic data. Q.Z. and R.K. conducted the PCoA analysis. M.L. performed the histology analysis. T.Z. conducted confocal microscopy analysis. B.S. collected and provided the intestinal polyps from human patients. E.Y., S.F., S.L. and E.G. provided scientific input. T.F., A.R.A., R.T.Y., M.D. and R.M.E. prepared the manuscript.

ACCESSION CODES

The RNA-seq data reported in this paper have been deposited in NCBI's Sequence Read Archive and are accessible through accession number SRP111558.

DECLARATION OF INTERESTS

S.F., C.L., R.T.Y., A.R.A., M.D. and R.M.E. are co-inventors of inventions related to certain FXR agonists.

The progression of colorectal cancer is fueled by bile acid-dependent inhibition of the receptor FXR.

growth and curtail CRC progression. This unexpected role for FXR in coordinating intestinal self-renewal with BA levels implicates FXR as a potential therapeutic target for CRC.

Graphical Abstract

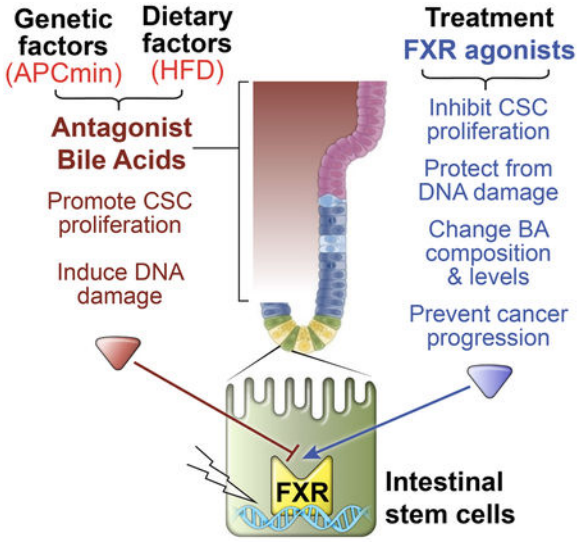

INTRODUCTION

Risk factors for colorectal cancer (CRC) include high fat diets, sedentary lifestyles, obesity, diabetes, and elevated serum levels of toxic bile acids (BAs) (de Aguiar Vallim et al., 2013; Degirolamo et al., 2011; Downes and Liddle, 2008; Font-Burgada et al., 2016; Kuipers et al., 2015; Thomas et al., 2008). While the majority of CRC cases are sporadic, ~85% of patients have mutations in the adenomatous polyposis coli (APC) gene, a crucial negative regulator of Wnt signaling (Fodde et al., 2001; Powell et al., 1992; Rajagopalan et al., 2003). The subsequent accumulation of mutations, including those activating the oncogene Kras and inactivating tumor suppressors including Smad4 and p53, drive a progression from adenoma to adenocarcinoma and ultimately, metastatic adenocarcinoma (Rajagopalan et al., 2003) (Dow et al., 2015; Drost et al., 2015; Kuipers et al., 2015; Ongen et al., 2014). Notably, restoring APC function can reestablish intestinal homeostasis *in vivo*, even in the presence of Kras and p53 mutations, confirming the critical regulatory role for APC (Dow et al., 2015).

$Lgr5^+$ intestinal stem cells (ISCs) are both the cell-of-origin for early neoplastic lesions caused by loss of the APC gene and necessary for metastasis (Barker et al., 2009). Located at the base of the crypt, precisely regulated cycles of renewal and differentiation of $Lgr5^+$ ISCs maintain the intestinal structure (Barker et al., 2009; Sato et al., 2009). This “bottom-top” cell hierarchy positively correlates with a Wnt signaling gradient, and inversely correlates with BA exposure. However, it remains unclear how erosion of the crypt/villi architecture and the subsequent increase in exposure of $Lgr5^+$ ISCs to BAs contribute to the initiation and progression of CRC (de Aguiar Vallim et al., 2013; Degirolamo et al., 2011; Thomas et al., 2008).

Dietary fatty acids have been implicated in enhancing the self-renewal capacity of ISCs and progenitor cells, as well as the tumor-initiating potential of cancer stem cells (CSCs) (Beyaz et al., 2016). However, high fat diets (HFDs) lead to commensurate increases in BAs, which are potent inducers of CRC malignancy (Degirolamo et al., 2011; Downes and Liddle, 2008). In the context of CRC, the secondary bile acids deoxycholic acid (DCA) and lithocholic acid (LCA) are of particular interest, as their hydrophobic nature promotes intestinal permeability and genotoxic effects (Bayerdorffer et al., 1995; Imray et al., 1992; Mahmoud et al., 1999).

The farnesoid X receptor (FXR) serves as a primary sensor of nutritional cues, translating stimuli into transcriptional programs (Degirolamo et al., 2011; Downes and Liddle, 2008; Forman et al., 1995; Makishima et al., 1999; Parks et al., 1999). In particular, FXR is the master regulator of BA homeostasis, governing synthesis, efflux, influx, and detoxification throughout the gut-liver axis (Thomas et al., 2008). Strong evidence suggests a role for FXR in intestinal tumorigenesis, with expression levels inversely correlating with CRC progression and malignancy (Anakk et al., 2011; De Gottardi et al., 2004; Degirolamo et al., 2011; Fu et al., 2016b; Maran et al., 2009; Modica et al., 2008; Selmin et al., 2016). Consistent with this, loss of FXR promotes the development of intestinal tumors in the $APC^{min/+}$ mouse model of CRC (Maran et al., 2009). While links between BAs, FXR, and CRC have been suggested, the underlying mechanisms remain unclear. Here, we establish that FXR controls $Lgr5^{+}$ intestinal stem cell proliferation. In CRC, we show that dietary and genetic risk factors converge to drive FXR-dependent $Lgr5^{+}$ CSC proliferation and disease progression. Conversely, activation of FXR in the intestine reduces disease severity to markedly increase survival.

RESULTS

HFD drives CRC progression in $APC^{min/+}$ mice

$APC^{min/+}$ mice develop multiple intestinal neoplasia predominantly within the ileum, however these lesions seldom progress past the adenoma stage (Powell et al., 1992). To understand the contributing effects of diet on tumor progression, we maintained wild type (WT) and $APC^{min/+}$ mice on a normal diet (ND) or HFD for 16 weeks. BAs measured down the digestive track of WT mice revealed HFD-induced increases in both the intestinal lumen and the adjacent tissues (Figure S1A). Marked increases in fecal BA, triglyceride (TG), and free fatty acid (FFA) levels were also evident in the intestine and the colon, though the absorption efficiency (TGs and BAs lost via the feces) was not significantly compromised (Figure S1B). In addition, intestinal morphological changes were observed in mice fed a HFD, including reduced villi length and deeper crypt invaginations (Figure 1A and S1C), along with a ~2.5 fold increase in intestinal permeability (Figure 1B). In $APC^{min/+}$ mice on ND, distorted epithelial growth (adenoma) attributed to dysregulated Wnt signaling was accompanied by compromised gut integrity (~7-fold increase in intestinal permeability compared to WT mice) (Figure 1B, 1C, and S1D). In addition, increased serum TGs and FFAs were suggestive of metabolic dysregulation (Figure S1E). Challenging $APC^{min/+}$ mice with a HFD led to epithelial hyper-proliferation, hyperplastic crypts, crypt-like invaginations in the villi throughout the ileum and colon, a ~14-fold increase in intestinal permeability

compared to WT mice, and further increases in serum TGs and FFAs (Figure 1B, 1C and S1E). In addition, increased serum levels of the CRC malignancy biomarker carcinoembryonic antigen (CEA) and the cancer antigen 19–9 (CA-19) support the notion that HFD promotes an adenoma-to-adenocarcinoma progression in $APC^{min/+}$ mice (Figure 1D and 1E).

The above data led us to consider that distortion of villus structure might increase the exposure of crypts to BAs and increase the progression from adenoma to adenocarcinoma in $APC^{min/+}$ mice. In support of this notion, marked increases were seen in total serum BAs in $APC^{min/+}$ mice on ND and HFD (~4-fold and ~10-fold, respectively) that included disproportionate increases in the levels of primary BAs (Figure 1F–1J, S1F, S1G and Table S1). Of particular interest, the levels of tauro-βMCA (T-βMCA) increased over 60-fold in $APC^{min/+}$ mice with HFD feeding (Figure 1K and 1L).

T-βMCA drives CRC progression in $APC^{min/+}$ mice

To explore the link between BA changes and carcinogenesis, BA levels were monitored in $APC^{min/+}$ mice during the progression from intestinal inflammation (6–7 weeks), to initial tumor development (8 weeks), and maximum tumor load (12–14 weeks) (Figure S2A–Figure S2D). Total bile acid levels, as well as levels of T-βMCA and DCA, tracked with tumor load, suggestive of a causal link (Figure 2A, 2B, S2C and S2D).

T-βMCA has previously been shown to inhibit the expression of FXR target genes (Sayin et al., 2013). Consistent with this, T-βMCA inhibited FXR reporter activity in the CRC cell line HT29 (EC_{50} ~10μM), compared to the synthetic FXR agonist GW4064 (Figure 2C and S2E). However, this inhibitory effect could be attenuated by the natural bile acid agonist chenodeoxycholic acid (CDCA) (Figure 2D and S2F). Given this ability to inhibit FXR signaling, we asked whether T-βMCA could promote tumor growth and proliferation. Indeed, a marked increase in proliferation was observed in the ileum of $APC^{min/+}$ mice after a single treatment with T-βMCA (400 mg/kg p.o. 12 hours prior to 50 mg/kg EdU injection, Figure 2E).

To determine whether T-βMCA alone is sufficient to recapitulate the adenocarcinoma-inducing effects of HFD *in vivo*, 10 week old $APC^{min/+}$ mice were administered T-βMCA via oral gavage (400 mg/kg twice a week for 6 weeks that increased serum T-βMCA levels to those seen in HFD-fed $APC^{min/+}$ mice, Figure S2G). Compared to vehicle, administration of T-βMCA markedly decreased intestinal integrity and accelerated tumor growth in the intestine and colon of $APC^{min/+}$ mice (Figure 2F and S2H). Histological analyses revealed invaginated (hyperplastic) crypts and shortened, branched villi with crypt-like pockets in the tumors, similar to the pathology observed in HFD-fed $APC^{min/+}$ mice. These pathological changes were accompanied with higher intestinal permeability and increased CA-19 and CEA levels (Figure 2G, 2H and S2I). T-βMCA treatment also significantly increased levels of serum cytokines, including IFN-γ, IL-6, and IL-17 (Figure S2J) (Devkota et al., 2012; Wang et al., 2014). Consistent with its antagonistic activity, T-βMCA treatment downregulated the expression of FXR target genes (*Shp*, *Ibabp*), as well as the expression of FXR itself, in colonic tumors (Figure 2I). Conversely, the expression of intestinal cancer and normal stem cell genes including *Ascl2, Myc, Lgr5*, *Olfm4* and *Tnfrsf19* were upregulated

in APC$^{min/+}$ mice treated with T-βMCA (Figure 2I). These findings imply that T-βMCA can effectively recapitulate the ability of HFD to promote CRC progression.

In order to confirm T-βMCA as a driver of cancer cell and cancer stem cell proliferation, we measured the effect of T-βMCA on their growth and proliferation. In CRC cell lines (HCT116 and HT29) and intestinal organoids derived from APC$^{min/+}$ mice, T-βMCA dose-dependently stimulated cell proliferation in an FXR-dependent manner (as measured by EdU incorporation, Figure S3A, S3B and S3C). To determine whether T-βMCA promoted proliferation in CSCs, we generated an intestinal stem cell-specific, inducible APC knockout mouse by crossing Lgr5-EGFP-IRES-CreERT2 and APC^{flox} mice (Lgr5-GFP, APC^{flox} mice). Intestinal organoids derived from tamoxifen-treated Lgr5-GFP, APC^{flox} mice were exposed to increasing doses of T-βMCA, and proliferation of stem cells determined by measuring the percentage of cells expressing high levels of GFP (GFP^{+}). Notably, T-βMCA treatment increased the percentage of GFP^{+} cells, suggesting that T-βMCA is able to drive CSC proliferation (Figure S3D). Supporting this notion, gene expression analysis of GFP^{+} cells following T-βMCA treatment revealed increased expression of intestinal stem cell markers (Figure S3E) (Sato et al., 2009; Schuijers et al., 2015; van der Flier et al., 2009b).

FXR regulates Lgr5^{+} cancer stem cell expansion

The observed inhibition of FXR signaling by T-βMCA led us to hypothesize that FXR activation may block CSC growth. While generally thought to be expressed only in the villi, our data and recently published single cell studies show FXR expression in Lgr5^{+} cells (Figure S4A and data not shown) (Haber et al., 2017). To explore this possibility, we utilized the intestinally-biased FXR agonist, FexD (Figure S4B). As a deuterated analog of Fexaramine, FexD retains the gut-restricted activity profile of Fexaramine while displaying improved *in vivo* efficacy (data not shown) (Downes et al., 2003; Fang et al., 2015).

In intestinal organoids generated from APC$^{min/+}$ mice on ND (an adenoma model of CRC), increased budding and branching was seen with T-βMCA treatment (Figure 3A and 3B), consistent with the induction of multiple genes associated with intestinal stem cell proliferation and the suppression of p53 pathway genes (Figure 3C and Table S2). FexD largely abrogated T-βMCA-induced organoid growth (reduced budding and branching) and blocked its effects on FXR target genes and intestinal stem cell marker gene expression in these organoids (Figure 3A and 3D). Similar suppressive effects of FexD on T-βMCA-induced cell growth were observed in three human colon cancer cell lines (data not shown). To confirm that FexD and T-βMCA act by FXR engagement in Lgr5^{+} cells, we treated organoids derived from Lgr5-GFP, APC^{flox} mice and subsequently sorted for Lgr5^{+} cells based on GFP fluorescence (Barker et al., 2009; Sato et al., 2009). T-βMCA dose-dependently increased Lgr5^{+} cell numbers and marker gene expression, whereas the addition of FexD counteracted these effects (Figure S4D and S4E) (Barker et al., 2009). Furthermore, the effects of both T-βMCA and FexD were largely abolished in organoids derived from APC$^{min/+}$ mice in which FXR had been conditionally deleted in ISCs (tamoxifen-treated APC$^{min/+}$/Lgr5-GFP/FXR^{flox} mice; Figure S4F–S4H) and FXR whole-body knockout mice (data not shown), establishing their FXR dependency. Collectively, these data demonstrate

that T-βMCA-mediated inhibition of FXR in intestinal stem cells drives organoid self-renewal; an effect that can be countered by treatment with the agonist FexD.

Organoids derived from $APC^{min/+}$ mice maintained on a HFD (an adenocarcinoma model of CRC) display increased growth rates compared to those derived from ND-fed mice, consistent with HFD promoting $Lgr5^{+}$ stem cell proliferation (Beyaz et al., 2016) (Figure 3E and S4I). To establish the utility of FXR as a therapeutic target in CRC, we evaluated the ability of structurally diverse FXR agonists to inhibit this more aggressive adenocarcinoma organoid model. Notably, the FXR agonists FexD, GW4064 and OCA (De Magalhaes Filho et al., 2016) each inhibited organoid growth, as did the chemotherapeutic drug 5-fluorouracil (5FU) (Figure 3E and 3F). Mechanistically, we found that the expression levels of intestinal stem cell genes including *Lgr5* and *Olfm4* were downregulated 50–90% upon agonist treatment (Figure 3G) (Sato et al., 2009; van der Flier et al., 2009a) whereas FXR target genes were prominently induced (Figure S4J). Interestingly, while FexD and OCA treatments both robustly suppressed stem cell gene expression, only FexD reduced the expression of the Wnt-dependent cancer stem cell gene *Ascl2* (Figure 3G) (Schuijers et al., 2015; van der Flier et al., 2009b). Furthermore, FexD and OCA treatments differentially regulated the induced intestinal stem cell genes (FexD suppressed ~120 of 150 genes, Figure 3H, 3I and Table S2), consistent with their action as selective FXR modulators (Schuijers et al., 2015). Moreover, treatment with FexD and OCA countered the observed suppression of many genes, most notably those involved in the p53 pathway, providing possible mechanistic insight into how FXR activation opposes colon cancer progression (Figure 3H–3J, S4K) (Dalerba et al., 2011; Drost et al., 2015; Fodde et al., 2001; Ongen et al., 2014; Rajagopalan et al., 2003).

Serum levels of DCA were also increased by HFD in $APC^{min/+}$ mice (Figure 1H, S1F and S1G). Given that DCA has been implicated in CRC growth and progression (Mahmoud et al., 1999; Pai et al., 2004), we explored its effects in intestinal organoids generated from $APC^{min/+}$ mice on ND. DCA induced intestinal CSC proliferation with similar efficacy as seen with T-βMCA (Figure S5A and S5B). The transcriptional consequences of DCA treatment overlapped those seen with T-βMCA, with intestinal and cancer stem cell signature genes being induced in a dose-dependent fashion (Figure S5C and S5D). Co-treatment of these organoids with FexD or OCA effectively blocked DCA-driven proliferation and largely inhibited the increases in intestinal and stem cell marker gene expression while robustly inducing FXR target genes (Figure S5B, S5D, and S5E). Collectively, these findings support a model in which increased levels of antagonistic BAs disrupt FXR signaling in $Lgr5^{+}$ intestinal stem cells resulting in CSC proliferation and an adenoma-to-adenocarcinoma progression. Importantly these effects can be largely suppressed by the FXR agonists, FexD and OCA (De Magalhaes Filho et al., 2016).

FXR guards stem cell proliferation and chromosome stability

Increased rates of growth and new organoid formation were seen when FXR was selectively deleted in ISCs (organoids generated from tamoxifen-treated $APC^{min/+}$/Lgr5-GFP/FXR^{flox} mice), implicating FXR as a regulator of ISC proliferation (Figure 4A and 4B). To explore this notion, we compared the transcriptomes of ISCs from WT/Lgr5-GFP, WT/Lgr5-

GFP/FXR^{flox}, APC$^{min/+}$/Lgr5-GFP, and APC$^{min/+}$/Lgr5-GFP/FXR^{flox} mice. ISCs (GFP+ high cells) were isolated from tamoxifen-treated mice (1 week after tamoxifen treatment), and the genome-wide transcriptional changes determined on sorted cells pooled from 6 mice. Consistent with FXR limiting stem cell proliferation, increased expression of proliferation marker genes was seen in both WT and APC$^{min/+}$ mice when FXR was deleted (Figure 4C and Table S3).

To mechanistically link increased levels of antagonistic BAs with disease progression, we initially explored the effects of T-βMCA and DCA on WNT signaling (Fodde et al., 2001). Notably, T-βMCA and DCA dose-dependently increased WNT signaling in HT29 and HCT116 cells, suggesting that the increased stem cell proliferation seen in organoid models was due to compounding effects of FXR antagonism and APC mutations on the WNT signaling pathway (Figure S5F and S5G). In contrast, the FXR agonists FexD and OCA inhibited basal WNT signaling (Figure 4D, S5F and S5G).

Building upon the 2-step hypothesis for colon cancer evolution, we next asked whether BA exposure induces the genetic instability required for malignant transformation (Fodde et al., 2001; Ongen et al., 2014; Rajagopalan et al., 2003). Indeed, treating APC$^{min/+}$ organoids with T-βMCA and DCA led to progressive increases in the levels of phosphorylated histone H2AX (p-H2AX), a marker of DNA double-strand breaks (Figure 4E and S5H) (Imray et al., 1992; Mahmoud et al., 1999). Concomitant increases in the levels of the DNA repair marker PARP (poly ADP-ribose polymerase) further support the finding that these BAs induce DNA damage (Figure S5I). In contrast, no increase in PARP was seen after OCA or FexD treatment, suggesting that the DNA damaging effects may be restricted to FXR antagonists (Figure S5I). Furthermore, prolonged exposure to DCA (APC$^{min/+}$ organoids cultured with DCA and passaged for over 10 generations) led to widespread chromosomal aberrations (Figure 4F and 4G).

Taken together, the above findings suggest that HFD-induced increases in BAs, specifically the FXR antagonists T-βMCA and DCA, provide the growth advantage (dysregulated WNT signaling) as well as induce the genetic instability necessary for malignant transformation of CRC (Fodde et al., 2001; Rajagopalan et al., 2003). Indeed, aberrant elevation of BAs on a background of chromosomal instability (induced by APC loss-of-function mutations) may be the critical step toward malignant transformation of adenomas.

Intestinally-restricted FXR agonist slows tumor progression

Based on the pro-tumorigenic effects of the FXR antagonists T-βMCA and DCA in APC$^{min/+}$ mice, we explored the potential for FXR activation to impede tumor progression (Modica et al., 2008). To this end, we treated APC$^{min/+}$ mice maintained on ND or HFD (models of adenoma and adenocarcinoma, respectively) with the FXR agonist FexD. In the adenoma model, mice were treated with vehicle or FexD (50 mg/kg daily oral gavage) beginning at the time of tumor initiation (8 weeks of age) for 8 or 12 weeks (Figure 5A). For HFD-fed APC$^{min/+}$ mice, treatment was started earlier (at 6 weeks) due to the more rapid disease progression in this adenocarcinoma model (Figure 5B). Activation of ileal FXR target genes by FexD was confirmed in all treatment groups (WT and APC$^{min/+}$ mice on ND and HFD, Figure 5C and 5D). FexD treatment reduced fecal bleeding and tumor-induced

weight loss in both the adenoma (Figure 5E and 5G) and adenocarcinoma (Figure 5F and 5H) models. Histological analyses showed reduced proliferation, improved nuclei morphology, as well as an increase in the number of differentiated cell types such as goblet cells in the intestines of FexD-treated mice (Figure 5I, 5J, S6A and S6B). Importantly, the average number of tumors was reduced by ~40% and ~25% in the FexD treated adenoma and adenocarcinoma models, respectively (Figure 5K, 5L, S6C–6F). In addition, FexD treatment improved the intestinal barrier function in both models as seen by the ~3 fold decrease in intestinal permeability (Figure 5M and 5N, S6G and S6H). Furthermore, FexD treatment reduced systemic inflammation, as seen by marked reductions in spleen weight and serum cytokine levels, most notably IL6, IL17a, and IL10 (Figure 5O–5R, S6I–S6N). Taken together, these findings demonstrate that selective activation of intestinal FXR retards the progression of adenomas and adenocarcinomas.

Activation of intestinal FXR improves BA homeostasis

To elucidate the mechanisms underlying the beneficial effects of intestinal FXR activation on disease progression, we determined the drug-induced changes in serum BAs. As expected, FexD robustly reduced total BA levels, most notably a ~10 fold reduction observed in HFD-fed $APC^{min/+}$ mice (Figure 6A–6D, Table S1). Importantly, the high levels of the FXR antagonists T-βMCA, DCA, and βMCA were markedly reduced with FexD treatment (Figure 6E–6F, Table S1). Principal coordinates analysis (PCoA) of BA compositions identified T-βMCA levels as a key distinguishing factor for FexD treatment, and T-βMCA as a primary factor contributing to tumor progression in $APC^{min/+}$ mice (Figure 6G). Together, these findings support the notion that T-βMCA is a major driver in the development of colon cancer, in part through its ability to dysregulate FXR signaling in intestinal stem cells.

FexD improves CRC survival

To mechanistically dissect the *in vivo* effects of FexD treatment, we determined the genome-wide expression changes induced in $APC^{min/+}$ mice on ND. As seen in the organoid studies, FexD treatment comprehensively reduced the expression of intestinal stem cell genes and increased the expression of genes in the p53 pathway (Figure 7A, 7B, S7A, and Table S3) (Dalerba et al., 2011; Drost et al., 2015; Fodde et al., 2001; Ongen et al., 2014; Rajagopalan et al., 2003). In addition, histological scoring revealed reduced tumor grades in the colon in the adenocarcinoma model ($APC^{min/+}$ mice on HFD), suggesting FexD delayed tumor progression in the treated mice (Figure 7C and Table S4). Consistent with these changes, survival studies revealed profound improvements upon FexD treatment. The median survival time was increased by 10 weeks in $APC^{min/+}$ mice on ND (23 to 33.5 weeks with 50 mg/kg/day FexD starting from 8 weeks of age, Figure 7D), while in the more aggressive adenocarcinoma model ($APC^{min/+}$ on HFD), FexD-treated mice survived an additional 6 weeks (18.5 to 24.5 weeks, Figure 7E).

To explore the potential relevance of these findings to human disease, we generated FexD expression signatures (30 most upregulated and 30 most downregulated genes) to interrogate a GEO database of 797 CRC patients. Parsing patients based on FexD expression signatures derived from $APC^{min/+}$ mice or organoids revealed pronounced survival advantages (Figure

7F, S7B, and Table S3). Furthermore, this survival advantage was evident in the subsets of Stage 3 and Stage 4 patients, as well as in patients in the TGCA database (data not shown). Moreover, expression of FXR has strong inverse correlation with that of LGR5 and ASCL2 in human CRC patients (Figure S7C and Table S3), consistent with a conserved role for FXR in the regulation of $Lgr5^+$ cell proliferation. Supporting these correlations, FXR antagonistic BAs (T-βMCA and DCA) and FXR agonist drugs (FexD), increased and decreased the expression of intestinal and cancer stem cell marker genes in organoids generated from the polyps collected from human CRC patients (Figure 7G).

DISCUSSION

The 2-step model of CRC proposes that loss of tumor suppressor function provides a survival advantage and facilitates clonal expansion. Here we identify FXR as a critical regulator of intestinal stem cell proliferation. While not considered a tumor suppressor, we show that disruption of FXR activity in intestinal stem cells is integral to disease progression (Figure 7H).

We show here that FXR is a point of convergence of heredity (H) and environmental (E) risk factors for CRC (re the Tomasetti and Vogelstein model). Our studies demonstrate that the APC mutation and high-fat diet independently and cooperatively increase the BA pool that results in the repression of FXR signaling in intestinal stem cells. Mechanistically, we identify T-βMCA and DCA, natural FXR antagonists upregulated in $APC^{min/+}$ mice, as potent drivers of CSC proliferation and capable of inducing DNA damage.

The high rate of intestinal stem cell divisions and the associated increased risk for DNA replication (R) errors has been implicated in the incidence of CRC (Tomasetti et al., 2017; Tomasetti and Vogelstein, 2015). Indeed, replacement of the intestinal epithelium requires the continuous renewal and differentiation of stem cells, a process regulated by the WNT signaling gradient and dependent upon the crypt-villus structure. Erosion of this structure not only disrupts the WNT gradient, but increases the exposure of crypt-resident $Lgr5^+$ cells to diet-induced cues including fatty acids and BAs, thereby increasing the possibility for malignant transformation. These findings support the importance of FXR in maintaining the crypt-villus structure, gut homeostasis and crypt integrity, as well as demonstrate how disabled FXR signaling contributes to the “bottom-up” model for CRC progression (Figure 7H and S7D).

Early screening combined with advances in surgical and adjuvant therapies have improved survival rates for CRC, but additional pharmacologic interventions are needed (Kuipers et al., 2015). Our findings identify FXR in the cancer stem cells as a potential therapeutic target for treating or preventing CRC. Indeed, we show that FexD, a gut-biased FXR agonist, delayed tumor progression and profoundly increased survival in $APC^{min/+}$ mouse models of adenoma and adenocarcinoma. Histological examination revealed that FexD impedes tumor progression at multiple stages: hyperplasia, micro-adenoma, adenoma and adenocarcinoma (Figure 7C), emphasizing the critical role of FXR in regulating CSCs. FXR actions in additional intestinal cell types such as endocrine cells, and its interaction with other signaling pathways may additionally contribute to its propitious role in maintaining crypt-

villus homeostasis (Gregorieff et al., 2015; Rodriguez-Colman et al., 2017; Sato et al., 2011). Thus, the re-establishment of FXR signaling not only restricts aberrant $Lgr5^+$ stem cell proliferation but also promotes gut health including restoring the intestinal barrier (De Gottardi et al., 2004; Modica et al., 2008) and BA homeostasis (Fu et al., 2016a; Parseus et al., 2017) (Figure 7D). Beyond its well-established role in regulating cytotoxicity of hydrophobic BAs, our study highlights the role of FXR in restricting the tumorigenesis of $Lgr5^+$ cells, which mediate the key adenoma-to-adenocarcinoma transformation. As one FXR agonist (OCA) has recently been approved and others are advancing in clinical trials for liver disease, a rapid translation of these findings into CRC patients is foreseeable.

STAR★METHODS

EXPERIMENTAL MODEL AND SUBJECT DETAILS

Animal Models—WT C57BL/6J (Cat # 000664), $APC^{min/+}$ (Cat # 002020), Lgr5-EGFP-IRES-creERT2 (Cat # 008875) and APC^{flox} mice (Cat # 009045) were purchased from Jackson Laboratory. FXR^{flox} mice were kindly provided by Dr. Pierre Chambon (University of Strasbourg, France) and maintained in the Evan's laboratory. All animal experiments were performed in the specific pathogen-free facilities at the Salk Institute following the Institutional Animal Care and Use Committee's guidelines.

Cell Lines—The human intestinal cancer cell lines HCT116, Caco2, HT29 and HEK293 were acquired from ATCC and cultured according to supplier's instructions.

METHOD DETAILS

Animal Studies—WT and $APC^{min/+}$ mice were maintained on normal chow diet (ND) or placed on a high-fat diet (HFD, Harlan Teklad, 60% of calories from fat) from 4 weeks of age. For early intervention experiments, Fexaramine D (FexD, 50mg/kg in corn oil) or vehicle was orally gavaged daily from 8 weeks of age for $APC^{min/+}$ mice on ND, or from 6 weeks for $APC^{min/+}$ mice on HFD. For tumor facilitation experiment, T-βMCA (400mg/kg in corn oil, Steraloids Inc, Cat # C1899–000) was orally gavaged twice a week for 6 weeks (Sayin et al., 2013). Cre induction in $Lgr5^+$-EGFP-IRES-creERT2, APC^{flox} and FXR^{flox} mice was performed by daily gavage of tamoxifen (10mg/kg) for five consecutive days (Barker et al., 2009).

Isolation and Generation of Mouse Intestinal Organoid—Intestines were washed in ice-cold PBS (Mg^{2+}/Ca^{2+}) (Corning, cat # 21–031-CM), containing 2% BSA (Gemini Bio-products, cat #900–208) and 2% antibiotic-antimycotic (Gibco, cat #15240–062). Crypts and villi were exposed by dicing the intestines into small pieces (1–2 cm long), followed by extensive washes to remove contaminants (Sato and Clevers, 2013). Then, GCDR (Gentle Cell Dissociation Reagent, Stem cell technologies, cat #7174) was used according to the manufacturer's instructions. Briefly, intestinal pieces were incubated on a gently rotating platform for 15 minutes. Subsequently, GCDR was removed and intestinal pieces were washed 3 times with PBS wash buffer with vigorous pipetting. The first and second fractions that usually contain loose pieces of mesenchyme and villi were not used. Fractions three and four containing the intestinal crypts were collected and pooled. Isolated crypts were filtered

through a 70μm nylon cell strainer (Falcon, cat #352350). Crypts were counted, then embedded in Matrigel (Corning, growth factor reduced, cat #354230), and cultured in Intesticult organoid growth medium (Stem cell technologies, cat #6005). For mouse colon organoids, additional Wnt3a (300ng/μl, R&D, cat #5036-WN-010) was added. Intestinal organoids used in this study were generated from $APC^{min/+}$ mice, Lgr5-GFP mice, Lgr5-GFP/APC^{flox} mice, Lgr5-GFP/FXR^{flox} mice, FXRKO mice.

Generation of Human Intestinal Organoid—Crypts were isolated from same-day Colonoscopy sample from patients with intestinal polyps. Human organoids generated from patient intestinal polyps were propagated and cultured similar as mouse intestinal organoids.

Fecal occult blood test (FOBT) and Histology examination—Fecal occult blood test was used to check for hidden blood in the feces (Beckman Coulter, Cat# 60151A). Swiss rolled sections of mouse intestine subjected to Hematoxylin and Eosin (H&E) staining were used for tumor stage examination (Pacific pathology, UCSD histology center). Two serial sections of each small intestine and colon were assessed histologically by a trained pathologist for intestinal tumors using the Pathology of mouse models of intestinal cancer: consensus report and recommendation (Boivin et al., 2003; Washington et al., 2013). Lesions of hyperplasia (Beyaz et al.), gastrointestinal intraepithelial neoplasia (or microadenoma, MC), low and high-grade adenomas (AD) and adenoadenocarcinoma (AC) were graded and counted on each section. Images were taken by Olympus Virtual Slide Microscope VS120.

Metabolite Measurement—Secondary metabolites such as Bile Acids, Triglyceride (TG) and Free Fatty Acids (FFAs) were measured in mouse serum and fecal samples by Total bile acid assay kit (Diazyme laboratories, cat #DZ042A-K), Triglyceride kit (Thermo scientific, cat #TR 22421/2780-250) and Free fatty acid kit (Bioassay systems, cat #50-489-265) according to manufacturer's instructions. Serum samples were diluted 1:5 with blank buffer, and calculations performed using standard controls included in the kit. For fecal samples, total bile acids and total fat were extracted from 500mg feces. TGs and FFAs were separately measured from total fat extracts.

Serum BA composition analysis—Authentic bile acid standards were purchased from Sigma, except glycolithocholic acid (GLCA), deoxycholic acid (DCA), HDCA, γ-MCA, β-MCA, α-MCA ω-MCA and tauro-β-muricholic acid (T-βMCA) which were purchased from Steraloids (Newport, RI), taurocholic acid (TCA) from Calbiochem (San Diego, CA), and the deuterated bile acid standards cholic-2,2,4,4-*d*4 acid, chenodeoxycholic-2,2,4,4-*d*4 acid, and lithocholic-2,2,4,4-*d*4 acid from C/D/N Isotopes (Quebec, Canada). Mouse serum (20μl) was protein precipitated with 80μl of ice cold acetonitrile containing 3.28ng of deuterated cholic acid (2, 2, 4, 4-d4 cholic acid) as an internal standard, vortexed 1 min and centrifuged at 10,000 rpm for 10 min at 4°C. Supern atants were evaporated under vacuum at room temperature and reconstituted in assay mobile phase and transferred to a 96-well plate for analysis. A Nextera UPLC (SHIMADZU, Kyoto, Japan) system used in combination with a Q-TRAP 5500 Mass Spectrometer (AB SCIEX, Toronto, Canada) with Analyst Software 1.6.2 (Kakiyama et al., 2014). Chromatographic separations were performed with an

ACQUITY (WATERS, Milford, MA) UPLC BEH C18 column (1.7microns, 2.1×100mm). The temperatures of the column and auto sampler were 65 degrees and 12 degrees, respectively. Sample injection was 1μL. The mobile phase consisted of 10% Acetonitrile and 10% Methanol in water containing 0.1% Formic Acid (Mobile Phase A) and 10% Methanol in Acetonitrile 0.1% Formic Acid (Mobile Phase B) delivered as a gradient: 0–5-min Mobile Phase B held at 22%; 5–12-min Mobile Phase B increased linearly to 60%, 12–15min Mobile Phase B increased linearly to 80% and 15–19min Mobile Phase B constant at 80% at a flow rate of 0.5ml/min. The mass spectrometer was operated in negative electro-spray mode working in the multiple reaction mode (MRM). Operating parameters were Curtain gas 30 psi; Ion spray voltage 4500 V; Temperature 550C; Ion Source Gas 1 60 psi; Ion Source Gas2 65 psi. Transition MRMs, de-clustering potential, entrance potentials and collision cell exit potentials were optimized using the Analyst software. Dwell times were 25 msec.

Cytokine and cancer tumor marker measurement—Serum levels of mouse cytokines were analyzed by the Luminex Bio-Plex system. The mouse cytokine 23-multiplex assay was carried out according to the manufacturer's instructions (Bio-Rad, cat #M60009RDPD). Specific cytokines such as IL-17, IL-6 and TNFα were measured with corresponding cytokine Elisa Kits (Life Technologies, cat # KMC3021, cat #KMC0061, cat #KMC3011). Tumor markers, Carcinoembryonic Antigen (CEA) (Lifespan Biosciences Inc, cat #LS-F5042) and Cancer Antigen 19–9 (CA 19–9) (Lifespan Biosciences Inc, cat #LS-F24309) were used to distinguish between benign and malignant tumors.

Cell viability assay and Cell Luciferase assay—FexD, OCA (Obeticholic acid), CDCA (Chenodeoxycholic acid) and GW4064 were dissolved in DMSO (FexD, in house production; OCA, GW4064, Selleck Chemical LLC). CellTiter-Glo Luminescent Cell Viability Assay Kit (Promega, cat #G7572) was used to assay cell viability after drug treatment. For luciferase assay, FXRE-Luc plasmids (FXR responsive element) were transfected into each cell line, then different drugs were added, and luciferase activities were measured by Dual-Luciferase reporter kit (Promega cat #PRE1910). Wnt signaling reporter assay by Cignal TCF/LEF Reporter (luc) Kit (Qiagen, CCS-018L) was used.

Viability Assays and RNA isolation of Mouse Organoids—Mouse organoids generated from mouse intestine and colon were treated with drugs either on day 2 or day 3 after plating to capture the early growth phase. Images of organoid morphology changes after drug treatment were taken with Olympus IX51 microscope. CellTiter-Glo Luminescent 3D Cell Viability Assay Kit (Promega, cat #G9683) was used to check the cell viability after 24 hrs of drug treatment. For RNA extraction, organoids were treated with drugs for 24–72 hrs, then directly lysed using TRIzol reagent (Ambion, cat #15596026), followed by a brief sonication (PowerLyzertm 24 MO Bio Laboratories Inc). RNeasy Mini Kit (Qiagen, cat #74106) was used for RNA extraction. Human organoids generated from patient intestinal polyps were propagated, and treated for 7 days with indicated drugs prior to RNA extraction.

Proliferation Assays of Mouse Organoids—Click-iT EdU-A647 flow cytometry kit (Life technologies, cat #C10424) and click-iT EdU-A647 imaging kit were used for cell

proliferation assays in both organoids and cell lines, counterstained with Hoechst. EdU was incubated for 1hr with organoids and cell lines before harvesting. For flow cytometry analysis, crypts were mechanically separated from the connective tissue by rigorous pipetting after incubation with GCDR (Stem cell technologies, cat #7174) for 15 mins. To obtain intestinal stem cells (ISCs) for sorting, pieces of intestinal sheets were incubated for 30 mins on a rocking platform. The cells were filtered through a 70-μm cell strainer (Falcon, cat #352350), then briefly dissociated with TrypLE Express enzyme (Gibco, cat #12604–013) into single cells. Sorting was done on a BD FACS cell sorter at the Salk and UCSD stem cell core. Specifically for Lgr5-GFP related mice, only GFP+ high cells were collected. The cells were collected in TRIzol reagent (Ambion, cat #15596026). Arcturus PicoPure RNA isolation kit (Applied Biosystems, cat #12204–01) was used for RNA extraction. Individual cells sorted from drug-treated organoids were isolated in a similar way with shorter incubation.

In vivo EdU assay—WT and $APC^{min/+}$ mice were gavaged with corn oil (vehicle control) with and without 400mg/kg of T-βMCA. 12 hrs later, 50 mg/kg EdU was injected intraperitoneally into the mice, according to Baseclick EdU in vivo kit's instructions. Small intestine and colon tissues were harvested at 4 hrs and 12 hrs. The slides were stained with EdU-Alexa 488, with DAPI-blue as a counter stain. Images were taken by Zeiss LSM 880 Rear Port Laser Scanning Confocal.

Gene Expression Analysis—Total RNA isolated from mouse intestine was perfused with RNAlater for 24h at 4 degree and then tissues were homogenized in TRIzol reagent (Ambion, cat #15596026) with beads using PowerLyzertm 24 (Mo Bio Laboratories Inc), then extracted by using RNeasy mini kit (Qiagen, cat #74106) as per the manufacturer's instructions. Total RNA isolated from mouse liver and intestinal segments was directly homogenized in TRIzol. cDNA was synthesized from 1 μg of DNase-treated total RNA using Bio-Rad iScript Reverse Transcription supermix (#1708841) and mRNA levels were quantified by quantitative PCR with Advanced Universal SyBr Green Supermix (Bio-Rad, cat #725271). All samples were run in technical triplicates and relative mRNA levels were calculated by using the standard curve methodology and normalized to 36B4. All primers are lists in Supplementary Table 5.

RNA-seq and Analysis—RNA quality was confirmed using the Agilent 2100 Bioanalyzer and RNA-seq libraries were prepared from three biological replicates for each experimental condition and sequenced on an Illumina HiSeq 2500, 4000, or NextSeq500 using barcoded multiplexing and a 100-bp read length. Image analysis and base calling were done with Illumina CASAVA-1.8.2. The quality of the reads was assessed with fastqc. Reads were mapped against the reference genome and transcript annotation (GRCm38.p6) using STAR (Dobin et al., 2013). RSEM (Li and Dewey, 2011) was utilized to quantify gene expression from BAM files. Differentially expressed genes (n = 3) were determined using rsem-generate-data-matrix and rsem-run-ebseq commands (Leng et al., 2013). For Figure 3C, genes were filtered with minimum 10 reads and fold changes were calculated from treatments (n=2). Top 30 up-regulated genes from the LGR5-ASCL2 signature were shown and top 30 down-regulated genes from the TP53 signature were shown in the heatmap. For

Figure 3H, 3I, 7A, S4K, S7A, row z-scores (n=3) were calculated from the matrix of normalized expression using R. For Figure 4C, GPF-positive cells pooled from 6 mice for each condition were sorted and RNA-seq was performed. For GSEA, normalized expression of gene matrix from RSEM results was used with previously reported gene signatures (Schuijers et al., 2015). GSEA was performed with the default setting (Subramanian et al., 2005). To generate heatmaps, z-scores were calculated from the matrix of normalized expression in each row using R.

Western blot analysis—Intestinal organoids were pooled from 3 wells (from 24-well plate), washed to remove matrigel and homogenized in Pierce RIPA Lysis and Extraction Buffer (ThermoFisher, cat # 89900), with freshly added Halt Protease Inhibitor Cocktail (100X) (ThermoFisher cat #78430). Crude lysates were centrifuged at 14,000g for 15 min and protein concentrations determined using Bio-Rad protein assay reagent. Samples were diluted in SDS sample buffer. Protein concentrations were measured by BCA (bicinchoninic acid assay) method. Bound proteins were resolved by SDS-PAGE and transferred to nitrocellulose membranes (Bio-Rad cat #170–4159). Individual proteins were detected with specific antibodies and visualized on film using horseradish peroxidase–conjugated secondary antibodies (Bio-Rad) and Western Lightning enhanced chemiluminescence (PerkinElmer Life Sciences). Antibodies to Phospho-Histone H2AX (Ser139) or γH2AX (20E3) Rabbit mAb (cat #9718), H2AX (cat #2595), were purchased from Cell Signaling and used at dilutions recommended by the manufacturer.

DNA Damage ELISA kits—APCmin organoids were treated with 10μM of adverse BAs (T-βMCA and DCA) and FXR agonist drugs (FexD and OCA) with incubation times of 5, 10, 15 and 30 mins to 1, 2, 4 up to 6 hour. DMSO was used as a negative control, and 5FU (Fluorouracil) as a positive control. Proteins were extracted from whole organoids with lysis buffer as described for western blots and measured with BCA assay. Extracted protein then used for PARP1 (poly ADP-ribose polymerase 1) ELISA Kit (LSBio, LS-F12266).

Chromosomal Damage Assay—Organoids generated from both WT and APCmin/+ mice were cultured and passaged in vehicle (DMSO) or 10 μM DCA for up to 10 generations. Prior to harvest, organoids were incubated in KaryoMAX™ Colcemid Solution (10μg/mL, Gibco) for 12–16 hrs, then single cells were resuspended in 0.075M KCl for 20 mins and fixed in Carnoy's solution. Cells were spread on slides and nuclei stained by DAPI prior to imaging using a Zeiss LSM 880 Rear Port Laser Scanning Confocal and Airyscan FAST Microscope.

PCoA Analysis—Statistical analyses of the metabolite profiles were performed using the QIIME package version 1.9.1. Specifically, a Bray-Curtis distance matrix was constructed based on the concentrations of the 23 metabolites in the 85 samples. Principal coordinates analysis (PCoA) was performed on the distance matrix to assess the clustering pattern of per-sample metabolite profiles. The result was visualized in Emperor (Caporaso et al., 2010). Permutational multivariate ANOVA was performed with 10,000 permutations using the adonis function of vegan 2.4–3, to test the significance of grouping $APC^{min/+}$ mice

samples based on either cohort (8 wks vs.12 wks) or drug (Veh vs. FexD). Mean distances between samples from different groups were also calculated.

Bioinformatic Human Survival Analysis.—In order to examine clinical relevance of gene signatures from organoids and mice, we conducted survival analysis with FexD-dependent genes. FexD-dependent genes (FDR<0.05 and Fold change > 1.5) were separated into UP and DOWN. To access and download large datasets, we utilized SurvExpress (Aguirre-Gamboa et al., 2013). Using combined GEO (n=808, GSE17536, GSE17538, GSE29621, GSE41258, GSE14333, GSE12945, E-GEOD-31595 used, survival data was available for 797 samples), coefficient scores were computed and the top 30 genes (negative scores for UP or positive scores for DOWN) were utilized. Patients were defined as high and low risk groups based on risk score (prognostic index). To generate Kaplan-Meier curves, functions from R packages (survival and survminer) were modified and utilized. For correlation study, we extracted expression of NR0B2, NR1H4, LGR5, and ASCL2 from the combined GEO dataset above that we used for survival analysis. Expression was normalized using scale function of R. Non-parametric Spearman correlation scores were calculated for statistics.

QUANTIFICATION AND STATISTICAL ANALYSIS

All statistical details of experiments are included in the Figure legends or specific Methods section. Band intensities were quantified with Fiji and normalized with internal control.

DATA AND SOFTWARE AVAILABILITY

The accession number for the RNA-seq data reported in this paper is NCBI SRA: SRP111558.

Supplementary Material

Refer to Web version on PubMed Central for supplementary material.

ACKNOWLEDGMENTS

We thank Z. Wei and W. Fan for scientific discussion, Y. Dai, J. Alvarez, H. Juguilon, L. Chong, and B. Collins for technical assistance, C. O'Connor, C. Fitzpatrick in Salk FACS core and UCSD FACS core for sorting the cells, David O'Keefe for editorial assistance, and L. Ong and C. Brondos for administrative assistance. This work was funded by grants from NIH (DK057978, HL105278, HL088093, ES010337), the Cancer Center (CA014195) and National Health and Medical Research Council of Australia Project Grants 512354 and 632886 (C.L. and M.D.), as well as the Leona M. and Harry B. Helmsley Charitable Trust (2017PG-MED001), Samuel Waxman Cancer Research Foundation and Ipsen/Biomeasure. T.F. is supported by a Hewitt Medical Foundation Fellowship and Salk Alumni Fellowship. R.M.E. and M.D. are supported in part by a Stand Up to Cancer Dream Team Translational Cancer Research Grant, a Program of the Entertainment Industry Foundation (SU2C-AACR-DT-20–16). R.M.E is an investigator of the Howard Hughes Medical Institute and March of Dimes Chair in Molecular and Developmental Biology at the Salk Institute.

REFERENCES

Aguirre-Gamboa R, Gomez-Rueda H, Martinez-Ledesma E, Martinez-Torteya A, Chacolla-Huaringa R, Rodriguez-Barrientos A, Tamez-Pena JG, and Trevino V (2013). SurvExpress: an online biomarker validation tool and database for cancer gene expression data using survival analysis. PLoS One 8, e74250. [PubMed: 24066126]

Anakk S, Watanabe M, Ochsner SA, McKenna NJ, Finegold MJ, and Moore DD (2011). Combined deletion of Fxr and Shp in mice induces Cyp17a1 and results in juvenile onset cholestasis. J Clin Invest 121, 86–95. [PubMed: 21123943]

Barker N, Ridgway RA, van Es JH, van de Wetering M, Begthel H, van den Born M, Danenberg E, Clarke AR, Sansom OJ, and Clevers H (2009). Crypt stem cells as the cells-of-origin of intestinal cancer. Nature 457, 608–611. [PubMed: 19092804]

Bayerdorffer E, Mannes GA, Ochsenkuhn T, Dirschedl P, Wiebecke B, and Paumgartner G (1995). Unconjugated secondary bile acids in the serum of patients with colorectal adenomas. Gut 36, 268–273. [PubMed: 7883228]

Beyaz S, Mana MD, Roper J, Kedrin D, Saadatpour A, Hong SJ, Bauer-Rowe KE, Xifaras ME, Akkad A, Arias E, et al. (2016). High-fat diet enhances stemness and tumorigenicity of intestinal progenitors. Nature 531, 53–58. [PubMed: 26935695]

Boivin GP, Washington K, Yang K, Ward JM, Pretlow TP, Russell R, Besselsen DG, Godfrey VL, Doetschman T, Dove WF, et al. (2003). Pathology of mouse models of intestinal cancer: consensus report and recommendations. Gastroenterology 124, 762–777. [PubMed: 12612914]

Caporaso JG, Kuczynski J, Stombaugh J, Bittinger K, Bushman FD, Costello EK, Fierer N, Pena AG, Goodrich JK, Gordon JI, et al. (2010). QIIME allows analysis of highthroughput community sequencing data. Nat Methods 7, 335–336. [PubMed: 20383131]

Dalerba P, Kalisky T, Sahoo D, Rajendran PS, Rothenberg ME, Leyrat AA, Sim S, Okamoto J, Johnston DM, Qian D, et al. (2011). Single-cell dissection of transcriptional heterogeneity in human colon tumors. Nat Biotechnol 29, 1120–1127. [PubMed: 22081019]

de Aguiar Vallim TQ, Tarling EJ, and Edwards PA (2013). Pleiotropic roles of bile acids in metabolism. Cell Metab 17, 657–669. [PubMed: 23602448]

De Gottardi A, Touri F, Maurer CA, Perez A, Maurhofer O, Ventre G, Bentzen CL, Niesor EJ, and Dufour JF (2004). The bile acid nuclear receptor FXR and the bile acid binding protein IBABP are differently expressed in colon cancer. Dig Dis Sci 49, 982–989. [PubMed: 15309887]

De Magalhaes Filho CD, Downes M, and Evans R (2016). Bile Acid Analog Intercepts Liver Fibrosis. Cell 166, 789. [PubMed: 27518554]

Degirolamo C, Modica S, Palasciano G, and Moschetta A (2011). Bile acids and colon cancer: Solving the puzzle with nuclear receptors. Trends Mol Med 17, 564–572. [PubMed: 21724466]

Devkota S, Wang Y, Musch MW, Leone V, Fehlner-Peach H, Nadimpalli A, Antonopoulos DA, Jabri B, and Chang EB (2012). Dietary-fat-induced taurocholic acid promotes pathobiont expansion and colitis in Il10−/− mice. Nature 487, 104–108. [PubMed: 22722865]

Dobin A, Davis CA, Schlesinger F, Drenkow J, Zaleski C, Jha S, Batut P, Chaisson M, and Gingeras TR (2013). STAR: ultrafast universal RNA-seq aligner. Bioinformatics 29, 15–21. [PubMed: 23104886]

Dow LE, O'Rourke KP, Simon J, Tschaharganeh DF, van Es JH, Clevers H, and Lowe SW (2015). Apc Restoration Promotes Cellular Differentiation and Reestablishes Crypt Homeostasis in Colorectal Cancer. Cell 161, 1539–1552. [PubMed: 26091037]

Downes M, and Liddle C (2008). Look who's talking: nuclear receptors in the liver and gastrointestinal tract. Cell Metab 7, 195–199. [PubMed: 18316024]

Downes M, Verdecia MA, Roecker AJ, Hughes R, Hogenesch JB, Kast-Woelbern HR, Bowman ME, Ferrer JL, Anisfeld AM, Edwards PA, et al. (2003). A chemical, genetic, and structural analysis of the nuclear bile acid receptor FXR. Mol Cell 11, 1079–1092. [PubMed: 12718892]

Drost J, van Jaarsveld RH, Ponsioen B, Zimberlin C, van Boxtel R, Buijs A, Sachs N, Overmeer RM, Offerhaus GJ, Begthel H, et al. (2015). Sequential cancer mutations in cultured human intestinal stem cells. Nature 521, 43–47. [PubMed: 25924068]

Fang S, Suh JM, Reilly SM, Yu E, Osborn O, Lackey D, Yoshihara E, Perino A, Jacinto S, Lukasheva Y, et al. (2015). Intestinal FXR agonism promotes adipose tissue browning and reduces obesity and insulin resistance. Nat Med 21, 159–165. [PubMed: 25559344]

Fodde R, Smits R, and Clevers H (2001). APC, signal transduction and genetic instability in colorectal cancer. Nat Rev Cancer 1, 55–67. [PubMed: 11900252]

Font-Burgada J, Sun B, and Karin M (2016). Obesity and Cancer: The Oil that Feeds the Flame. Cell Metab 23, 48–62. [PubMed: 26771116]

Forman BM, Goode E, Chen J, Oro AE, Bradley DJ, Perlmann T, Noonan DJ, Burka LT, McMorris T, Lamph WW, et al. (1995). Identification of a nuclear receptor that is activated by farnesol metabolites. Cell 81, 687–693. [PubMed: 7774010]

Fu T, Choi S-E, Kim D-H, Seok S, Suino-Powell KM, Xu HE, and Kemper JK (2012). Aberrantly elevated microRNA-34a in obesity attenuates hepatic responses to FGF19 by targeting a membrane coreceptor β-Klotho. Proceedings of the National Academy of Sciences 109, 16137–16142.

Fu T, Kim YC, Byun S, Kim DH, Seok S, Suino-Powell K, Xu HE, Kemper B, and Kemper JK (2016a). FXR Primes the Liver for Intestinal FGF15 Signaling by Transient Induction of beta-Klotho. Mol Endocrinol 30, 92–103. [PubMed: 26505219]

Fu T, Zhao X, and Evans RM (2016b). Liver Cancer Checks in When Bile Acid Clocks Out. Cancer Cell 30, 827–828. [PubMed: 27960079]

Gregorieff A, Liu Y, Inanlou MR, Khomchuk Y, and Wrana JL (2015). Yap-dependent reprogramming of Lgr5(+) stem cells drives intestinal regeneration and cancer. Nature 526, 715–718. [PubMed: 26503053]

Haber AL, Biton M, Rogel N, Herbst RH, Shekhar K, Smillie C, Burgin G, Delorey TM, Howitt MR, Katz Y, et al. (2017). A single-cell survey of the small intestinal epithelium. Nature 551, 333–339. [PubMed: 29144463]

Imray CH, Radley S, Davis A, Barker G, Hendrickse CW, Donovan IA, Lawson AM, Baker PR, and Neoptolemos JP (1992). Faecal unconjugated bile acids in patients with colorectal cancer or polyps. Gut 33, 1239–1245. [PubMed: 1427378]

Kakiyama G, Muto A, Takei H, Nittono H, Murai T, Kurosawa T, Hofmann AF, Pandak WM, and Bajaj JS (2014). A simple and accurate HPLC method for fecal bile acid profile in healthy and cirrhotic subjects: validation by GC-MS and LC-MS. J Lipid Res 55, 978–990. [PubMed: 24627129]

Kuipers EJ, Grady WM, Lieberman D, Seufferlein T, Sung JJ, Boelens PG, van de Velde CJ, and Watanabe T (2015). Colorectal cancer. Nat Rev Dis Primers 1, 15065. [PubMed: 27189416]

Leng N, Dawson JA, Thomson JA, Ruotti V, Rissman AI, Smits BM, Haag JD, Gould MN, Stewart RM, and Kendziorski C (2013). EBSeq: an empirical Bayes hierarchical model for inference in RNA-seq experiments. Bioinformatics 29, 1035–1043. [PubMed: 23428641]

Li B, and Dewey CN (2011). RSEM: accurate transcript quantification from RNA-Seq data with or without a reference genome. BMC Bioinformatics 12, 323. [PubMed: 21816040]

Mahmoud NN, Dannenberg AJ, Bilinski RT, Mestre JR, Chadburn A, Churchill M, Martucci C, and Bertagnolli MM (1999). Administration of an unconjugated bile acid increases duodenal tumors in a murine model of familial adenomatous polyposis. Carcinogenesis 20, 299–303. [PubMed: 10069468]

Makishima M, Okamoto AY, Repa JJ, Tu H, Learned RM, Luk A, Hull MV, Lustig KD, Mangelsdorf DJ, and Shan B (1999). Identification of a nuclear receptor for bile acids. Science 284, 1362–1365. [PubMed: 10334992]

Maran RR, Thomas A, Roth M, Sheng Z, Esterly N, Pinson D, Gao X, Zhang Y, Ganapathy V, Gonzalez FJ, et al. (2009). Farnesoid X receptor deficiency in mice leads to increased intestinal epithelial cell proliferation and tumor development. J Pharmacol Exp Ther 328, 469–477. [PubMed: 18981289]

Modica S, Murzilli S, Salvatore L, Schmidt DR, and Moschetta A (2008). Nuclear bile acid receptor FXR protects against intestinal tumorigenesis. Cancer Res 68, 9589–9594. [PubMed: 19047134]

Ongen H, Andersen CL, Bramsen JB, Oster B, Rasmussen MH, Ferreira PG, Sandoval J, Vidal E, Whiffin N, Planchon A, et al. (2014). Putative cis-regulatory drivers in colorectal cancer. Nature 512, 87–90. [PubMed: 25079323]

Pai R, Tarnawski AS, and Tran T (2004). Deoxycholic acid activates beta-catenin signaling pathway and increases colon cell cancer growth and invasiveness. Mol Biol Cell 15, 2156–2163. [PubMed: 15004225]

Parks DJ, Blanchard SG, Bledsoe RK, Chandra G, Consler TG, Kliewer SA, Stimmel JB, Willson TM, Zavacki AM, Moore DD, et al. (1999). Bile acids: natural ligands for an orphan nuclear receptor. Science 284, 1365–1368. [PubMed: 10334993]

Parseus A, Sommer N, Sommer F, Caesar R, Molinaro A, Stahlman M, Greiner TU, Perkins R, and Backhed F (2017). Microbiota-induced obesity requires farnesoid X receptor. Gut 66, 429–437. [PubMed: 26740296]

Powell SM, Zilz N, Beazer-Barclay Y, Bryan TM, Hamilton SR, Thibodeau SN, Vogelstein B, and Kinzler KW (1992). APC mutations occur early during colorectal tumorigenesis. Nature 359, 235–237. [PubMed: 1528264]

Rajagopalan H, Nowak MA, Vogelstein B, and Lengauer C (2003). The significance of unstable chromosomes in colorectal cancer. Nat Rev Cancer 3, 695–701. [PubMed: 12951588]

Rodriguez-Colman MJ, Schewe M, Meerlo M, Stigter E, Gerrits J, Pras-Raves M, Sacchetti A, Hornsveld M, Oost KC, Snippert HJ, et al. (2017). Interplay between metabolic identities in the intestinal crypt supports stem cell function. Nature 543, 424–427. [PubMed: 28273069]

Sato T, and Clevers H (2013). Growing self-organizing mini-guts from a single intestinal stem cell: mechanism and applications. Science 340, 1190–1194. [PubMed: 23744940]

Sato T, van Es JH, Snippert HJ, Stange DE, Vries RG, van den Born M, Barker N, Shroyer NF, van de Wetering M, and Clevers H (2011). Paneth cells constitute the niche for Lgr5 stem cells in intestinal crypts. Nature 469, 415–418. [PubMed: 21113151]

Sato T, Vries RG, Snippert HJ, van de Wetering M, Barker N, Stange DE, van Es JH, Abo A, Kujala P, Peters PJ, et al. (2009). Single Lgr5 stem cells build crypt-villus structures in vitro without a mesenchymal niche. Nature 459, 262–265. [PubMed: 19329995]

Sayin SI, Wahlstrom A, Felin J, Jantti S, Marschall HU, Bamberg K, Angelin B, Hyotylainen T, Oresic M, and Backhed F (2013). Gut microbiota regulates bile acid metabolism by reducing the levels of tauro-beta-muricholic acid, a naturally occurring FXR antagonist. Cell Metab 17, 225–235. [PubMed: 23395169]

Schuijers J, Junker JP, Mokry M, Hatzis P, Koo BK, Sasselli V, van der Flier LG, Cuppen E, van Oudenaarden A, and Clevers H (2015). Ascl2 acts as an R-spondin/Wnt-responsive switch to control stemness in intestinal crypts. Cell Stem Cell 16, 158–170. [PubMed: 25620640]

Selmin OI, Fang C, Lyon AM, Doetschman TC, Thompson PA, Martinez JD, Smith JW, Lance PM, and Romagnolo DF (2016). Inactivation of Adenomatous Polyposis Coli Reduces Bile Acid/Farnesoid X Receptor Expression through Fxr gene CpG Methylation in Mouse Colon Tumors and Human Colon Cancer Cells. J Nutr 146, 236–242. [PubMed: 26609171]

Subramanian A, Tamayo P, Mootha VK, Mukherjee S, Ebert BL, Gillette MA, Paulovich A, Pomeroy SL, Golub TR, Lander ES, et al. (2005). Gene set enrichment analysis: a knowledge-based approach for interpreting genome-wide expression profiles. Proc Natl Acad Sci U S A 102, 15545–15550. [PubMed: 16199517]

Thomas C, Pellicciari R, Pruzanski M, Auwerx J, and Schoonjans K (2008). Targeting bile-acid signalling for metabolic diseases. Nat Rev Drug Discov 7, 678–693. [PubMed: 18670431]

Tomasetti C, Li L, and Vogelstein B (2017). Stem cell divisions, somatic mutations, cancer etiology, and cancer prevention. Science 355, 1330–1334. [PubMed: 28336671]

Tomasetti C, and Vogelstein B (2015). Cancer etiology. Variation in cancer risk among tissues can be explained by the number of stem cell divisions. Science 347, 78–81. [PubMed: 25554788]

van der Flier LG, Haegebarth A, Stange DE, van de Wetering M, and Clevers H (2009a). OLFM4 is a robust marker for stem cells in human intestine and marks a subset of colorectal cancer cells. Gastroenterology 137, 15–17. [PubMed: 19450592]

van der Flier LG, van Gijn ME, Hatzis P, Kujala P, Haegebarth A, Stange DE, Begthel H, van den Born M, Guryev V, Oving I, et al. (2009b). Transcription factor achaete scute-like 2 controls intestinal stem cell fate. Cell 136, 903–912. [PubMed: 19269367]

Wang K, Kim MK, Di Caro G, Wong J, Shalapour S, Wan J, Zhang W, Zhong Z, Sanchez-Lopez E, Wu LW, et al. (2014). Interleukin-17 receptor a signaling in transformed enterocytes promotes early colorectal tumorigenesis. Immunity 41, 1052–1063. [PubMed: 25526314]

Washington MK, Powell AE, Sullivan R, Sundberg JP, Wright N, Coffey RJ, and Dove WF (2013). Pathology of rodent models of intestinal cancer: progress report and recommendations. Gastroenterology 144, 705–717. [PubMed: 23415801]

Highlights

- Genetic and dietary risk factors for colorectal cancer converge on the BA-FXR axis
- FXR controls the proliferation of $Lgr5^+$ intestinal stem cells
- FXR agonists curtail colorectal cancer progression

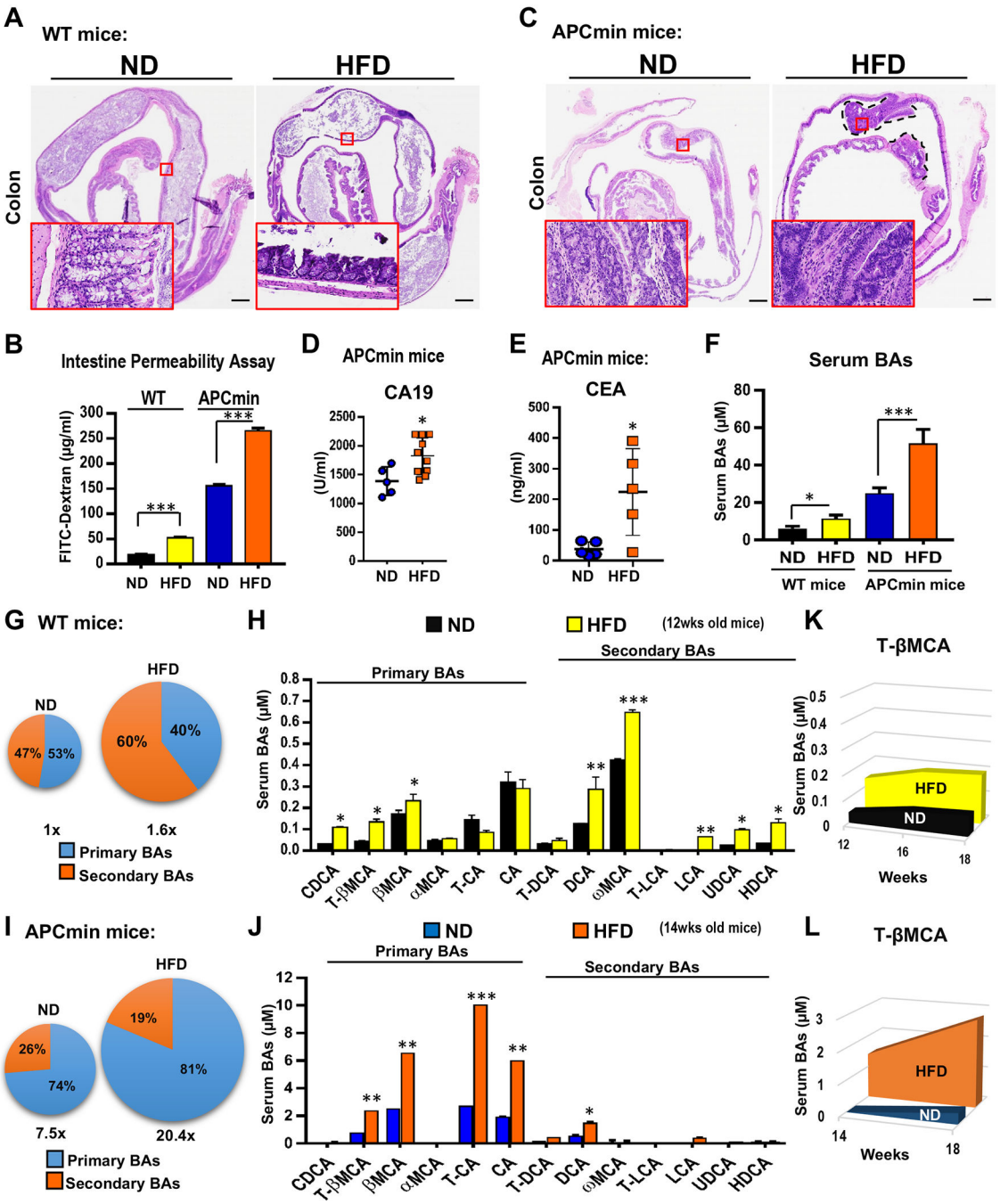

Figure 1. HFD drives adenoma-adenocarcinoma progression in APC$^{min/+}$ mice

Wild-type (WT) and APC$^{min/+}$ mice were maintained on normal-chow diet (ND) or high-fat diet (HFD) from 4 weeks of age.

(**A, C**) H&E staining of colons, with inset magnification of the epithelium. Large tumors are demarcated by dashed lines. Scale bar 1mm.

(**B**) Intestinal permeability, measured by oral FITC-Dextran leakage into blood, in WT and APC$^{min/+}$ mice (16 week old) maintained on ND or HFD for 12 weeks.

(**D-E**) Prognostic tumor marks of colon cancer, serum cancer antigen 19–9 (CA19) and carcinoembryonic antigen (CEA) in $APC^{min/+}$ mice.
(**F**) Total serum BA levels.
(**G**) Serum BA composition and (**H**) individual BAs levels in WT mice maintained on ND and HFD for 8 weeks.
(**I**) Serum BA composition and (**J**) individual BA levels of $APC^{min/+}$ mice maintained on ND and HFD for 10 weeks.
(**K-L**) Temporal changes in serum T-βMCA levels in WT and $APC^{min/+}$ mice on ND and HFD.
Data represent the mean ± SEM. *p<0.05; **p<0.01; ***p<0.005, Student's unpaired t-test.

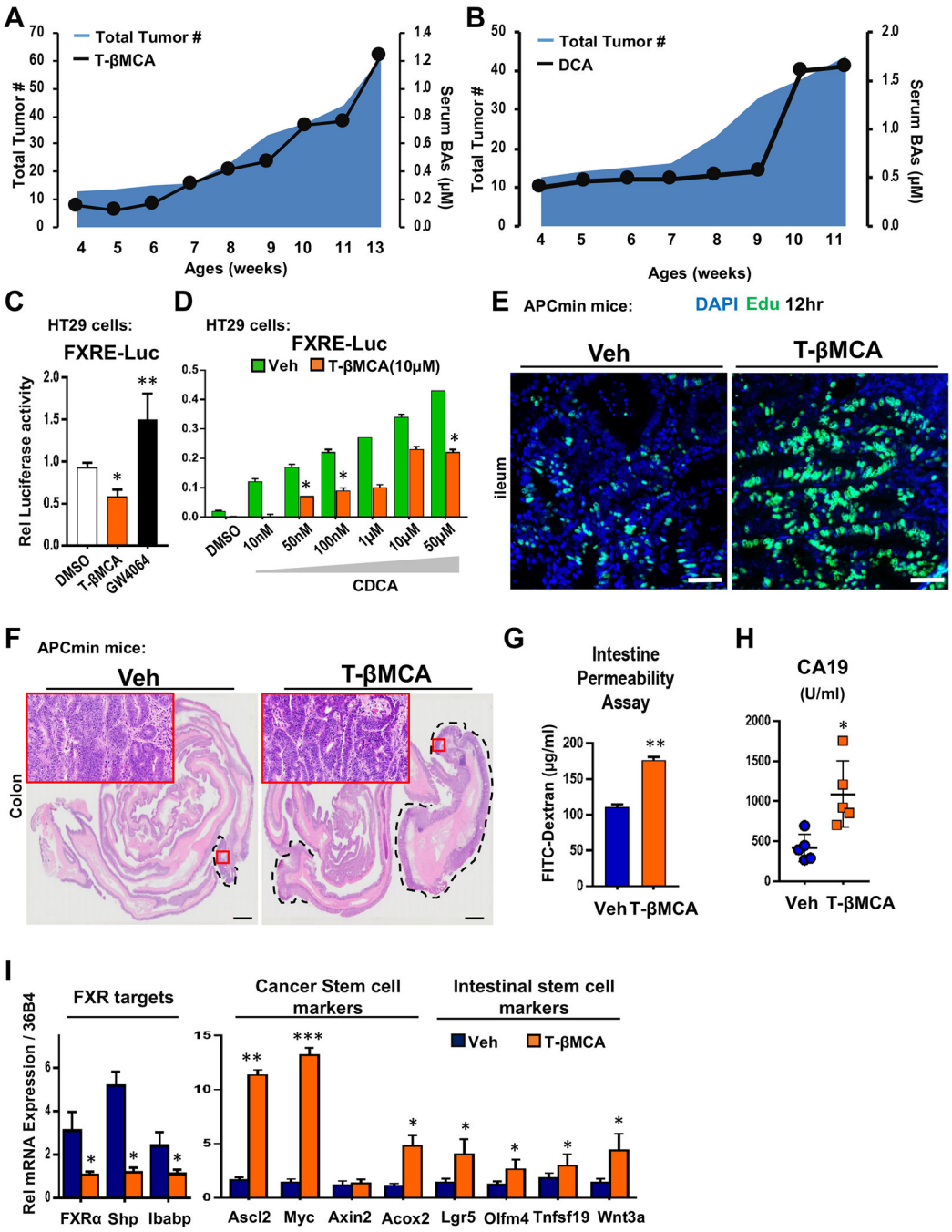

Figure 2. T-βMCA promotes CRC progression

(A-B) Temporal changes in intestinal tumor burden and serum T-βMCA and DCA levels. (**C**) Luciferase activity in HT29 cells expressing a luciferase reporter gene functionally linked to an FXR-responsive element (FXRE-Luc) upon exposure to T-βMCA or the FXR agonist GW4064, and (**D**) T-βMCA (10μM) in combination with CDCA (10nM to 50μM). (**E**) Ileal proliferation in ND-fed APC$^{min/+}$ mice 12 hours after T-βMCA (400mg/kg p.o.) or vehicle (corn oil) administration (EdU incorporation, green; DAPI, blue. Scale bar 50μm).

(**F**) H&E staining of colons and magnifications of the epithelium of $APC^{min/+}$ mice on ND treated with T-βMCA (400mg/kg p.o.) or Vehicle (corn oil) twice a week from 8 weeks of age. Tumors are outlined. Scale bar 1mm.

(**G-H**) Intestinal permeability and serum CA19 levels in $APC^{min/+}$ mice treated with T-βMCA or Vehicle.

(**I**) Relative expression of FXR target genes, and cancer and intestinal stem cell marker genes in tumors from $APC^{min/+}$ mice treated with Vehicle or T-βMCA (400 mg/kg twice a week for 6 weeks).

Data represent the mean ± SEM. *p<0.05; **p<0.01; ***p<0.005. Student's unpaired t-test.

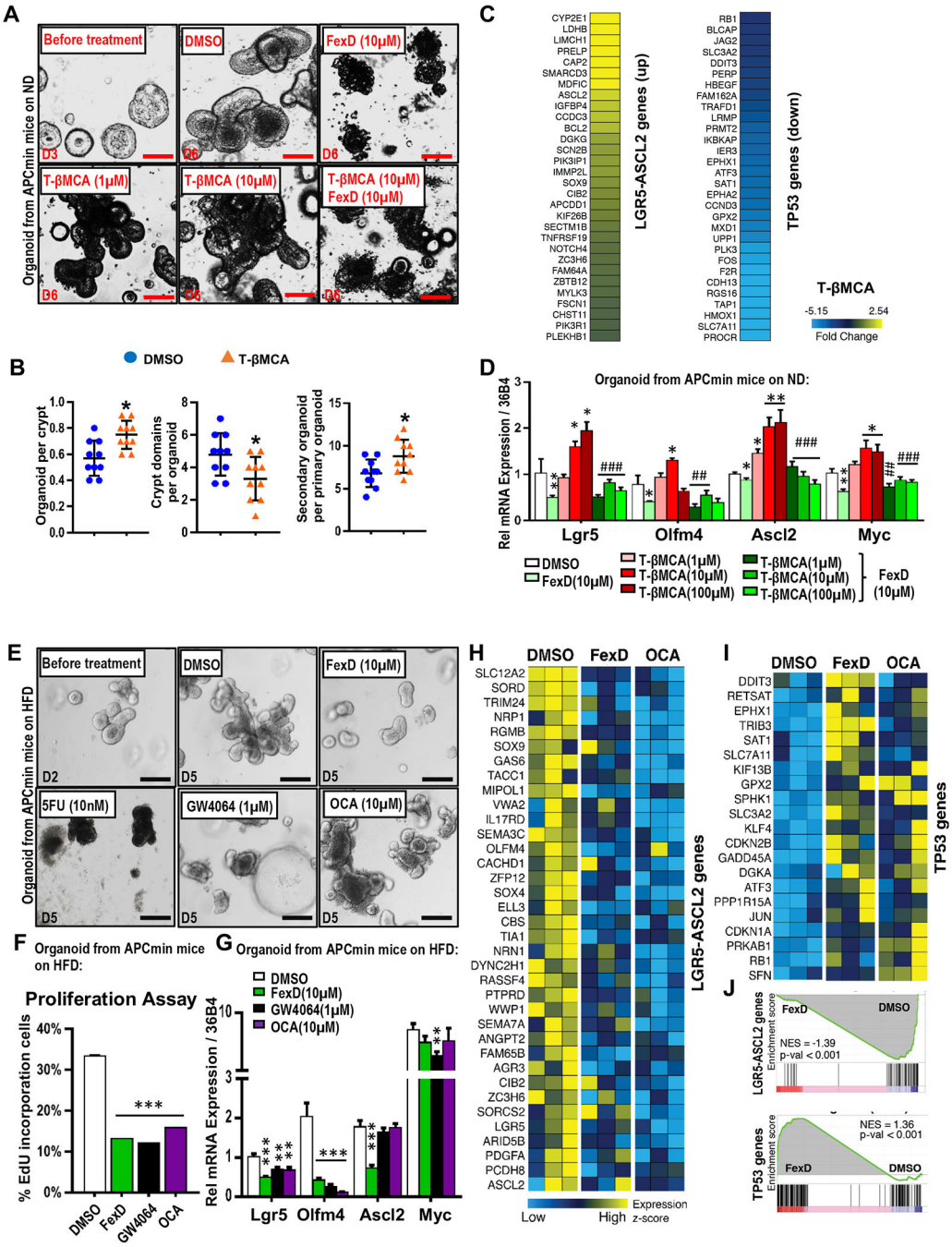

Figure 3. FXR regulates Lgr5^{+} cancer stem cell expansion

(**A**) Brightfield images of organoids generated from APC$^{min/+}$ mice on ND, treated from days 3–6 with vehicle (DMSO), T-βMCA, FexD, and T-βMCA+ FexD. Scale bar 50μm.

(**B**) Quantification of organoid budding in (A).

(**C**) Heatmap of stem cell marker gene expression in DMSO vs T-βMCA-treated organoids from (**A**).

(**D**) Expression of intestinal stem cell (Lgr5-Ascl2) and p53 pathway marker genes in APC$^{min/+}$ organoids treated with T-βMCA with and without concurrent FexD treatment (*

statistically different from vehicle; # statistically different from equivalent T-βMCA treatment).

(**E-G**) Organoids generated from $APC^{min/+}$ mice on HFD, treated with FXR agonists (FexD, OCA and GW4064) or 5-Fluorouracil (5-FU) from days 2–5.

(**E**) Brightfield images, scale bar 100μm.

(**F**) Proliferation of organoids measured by EdU incorporation. (**G**) Stem cell marker gene expression after indicated treatments.

(**H-I**) Heatmaps of changes in (**H**) stem cell gene signature (Lgr5-Ascl2) and (**I**) P53 pathway genes in $APC^{min/+}$ organoids after indicated treatments. Three representative replicates are shown.

(**J**) GSEA of FexD-induced changes in the stem cell signature (Lgr5-Ascl2) and P53 pathway genes.

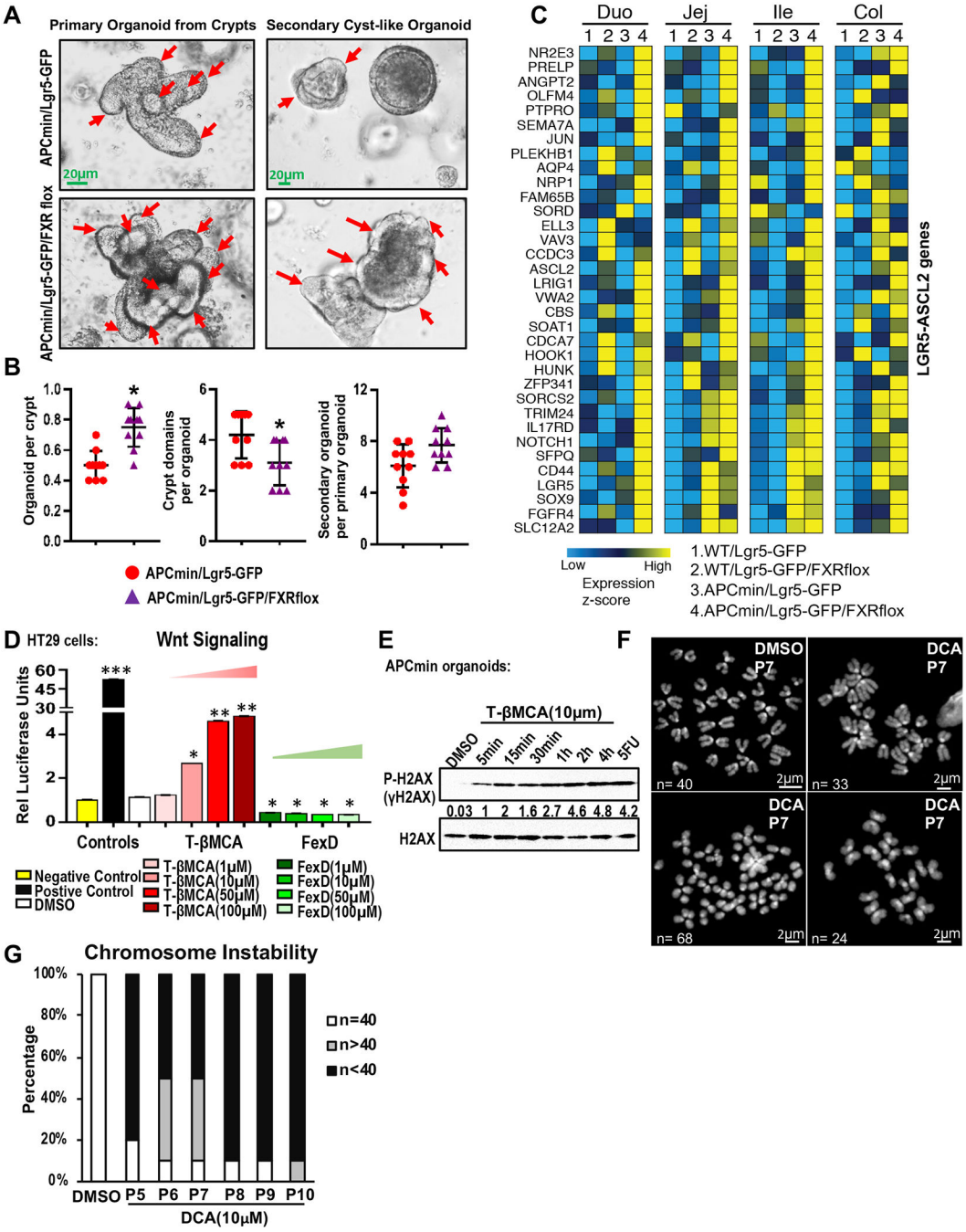

Figure 4. FXR guards stem cell proliferation and chromosome stability

(**A**) Brightfield images of primary and secondary organoids generated from APC$^{min/+}$/Lgr5-GFP and APC$^{min/+}$/Lgr5-GFP/FXR^{flox} mice. Arrows indicate crypt domains. Scale bar 20μm.

(**B**) Quantification of crypts and secondary organoid formation in organoids from (A).

(**C**) Heatmap showing relative gene expression in ISCs isolated from intestinal segments from APC$^{min/+}$/Lgr5-GFP, APC$^{min/+}$/Lgr5-GFP/FXR^{flox}, WT/Lgr5-GFP, and WT/Lgr5-

GFP/FXR^{flox} mice (Lgr5-GFP+high cells -ISCs, were isolated were pooled from 6 mice 1 week after tamoxifen treatment).

(**D**) Luciferase activity in HT29 cells expressing a WNT signaling luciferase reporter upon treatment with FexD and T-βMCA.

(**E**) Western blot of phosphorylated H2AX (pH2AX), a marker of DNA damage, in APC$^{min/+}$ organoids at indicated times after exposure to T-βMCA. Relative pH2AX levels measured by Image J are indicated.

(**F**) Representative images of chromosomes in organoids (from APC$^{min/+}$ mice) treated with DCA (10μm) or DMSO (control) for 7 passages.

(**G**) Quantification of chromosome numbers from passages 5 to 10 of organoids in (F). Data represent the mean ± SEM. *, $^{\#}$ p<0.05; **, $^{\#\#}$ p<0.01; ***, $^{\#\#\#}$ p<0.005. Student's unpaired t-test.

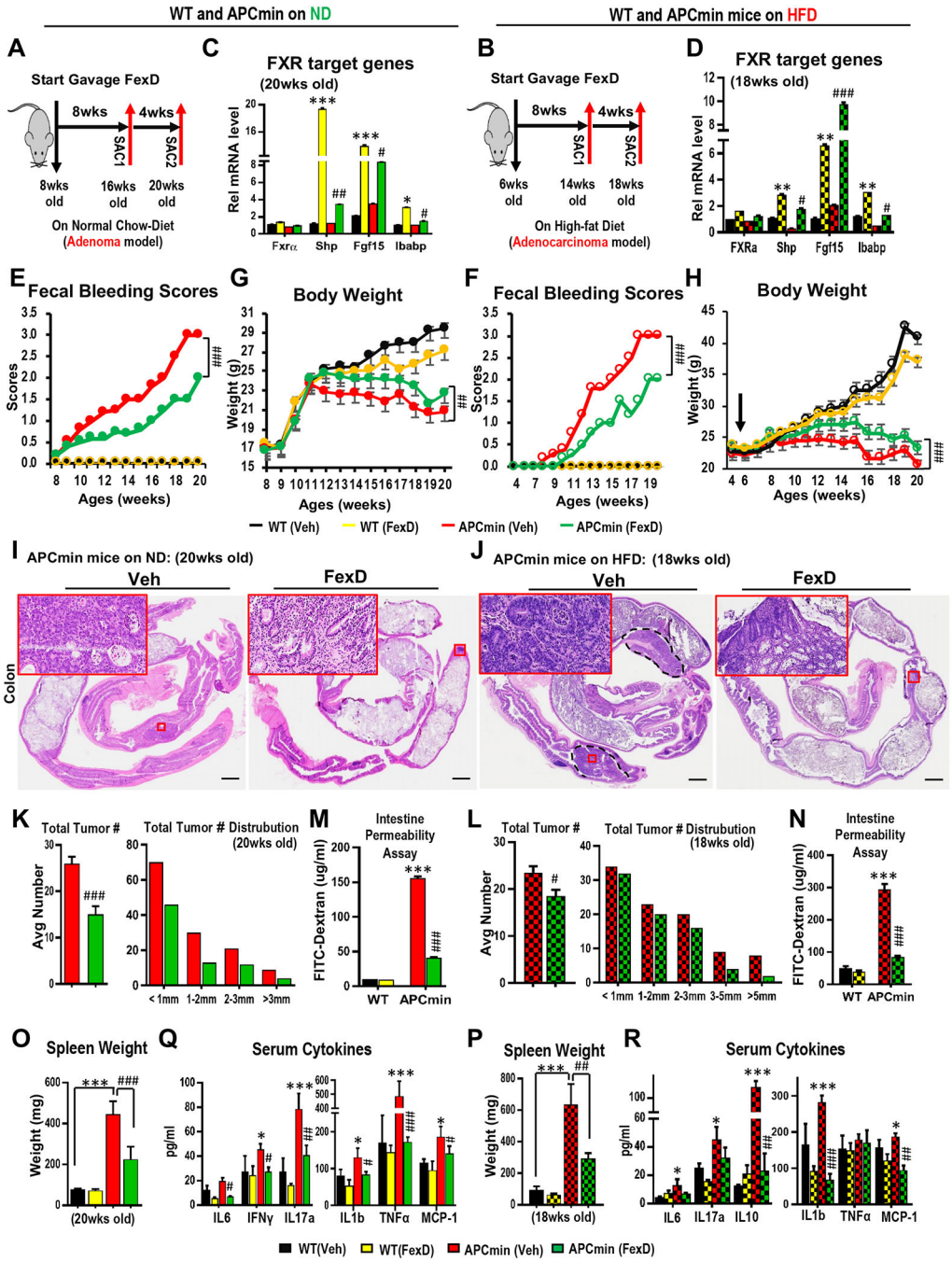

Figure 5. Intestinally-restricted FXR agonism slows tumor progression

(**A, B**) Schematics of FexD treatment (50mg/kg/day p.o.) of WT and APC$^{min/+}$ mice on ND and HFD. Mice were fed HFD from 4 weeks.

(**C, D**) Relative expression of FXR target genes (Shp, Fgf15 and Ibabp) in vehicle-treated WT (black), FexD-treated WT (yellow), vehicle-treated APC$^{min/+}$ (red), and FexD-treated APC$^{min/+}$ (green) mice.

(**E, F**) Progressive changes in fecal bleeding scores measured by fecal occult blood test, and (**G, H**) body weights in above treatment groups.

(**I, J**) Representative H&E staining of colons from 20 week old ND and 18 week old HFD fed mice as described above, with large tumors outlined. Enlarged images show the detailed structure. Scale bar 1mm.

(**K, L**) Average tumor burden and tumor size distribution of mice in above treatment groups.

(**M, N**) Intestinal permeability measured by FITC-Dextran of mice in above treatment groups.

(**O-R**) Spleen weight and serum cytokine levels in mice in above treatment groups.

Data represent the mean ± SEM. * statistically different from WT mice on ND; $^{\#}$ statistically different from $APC^{min/+}$ on ND. *, $^{\#}$ $p<0.05$; **, $^{\#\#}$ $p<0.01$; ***, $^{\#\#\#}$ $p<0.005$. Student's unpaired t-test.

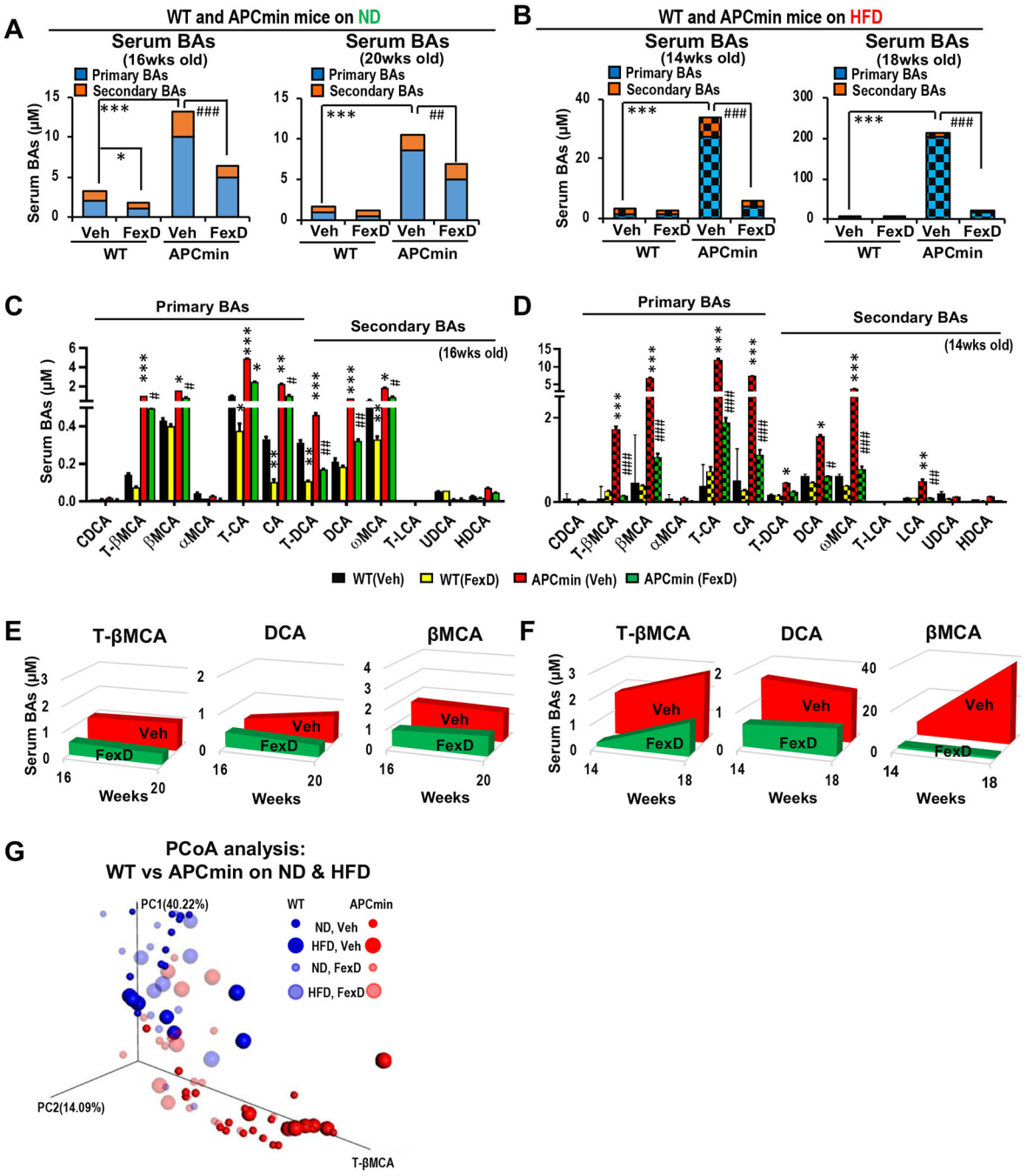

Figure 6. Activation of intestinal FXR improves BA homeostasis

WT and APC$^{min/+}$ mice on ND and HFD were treated as described in Figure 5A and B. Experimental schemes of Vehicle (black) and FexD-treated (50mg/kg/day p.o., yellow) WT and Vehicle (red) and FexD-treated (green) APC$^{min/+}$ mice as described in Figure 5A, C.

(**A, B**) Total primary and secondary serum BA levels during disease progression in mice described above.

(**C, D**) Individual serum BA levels in 16 week old ND-fed and 14 week old HFD-fed mice after indicated treatments.

(**E, F**) Temporal changes in serum T-βMCA, DCA and βMCA levels.

(**G**) Principal coordinates analysis (PCoA) of the effects of genotype, diet, and FexD treatment on BA compositions.

Data represent the mean ± SEM. * statistically different from WT mice on ND; # statistically different from $APC^{min/+}$ on ND. *, # $p<0.05$; **, ## $p<0.01$; ***, ### $p<0.005$. Student's unpaired t-test.

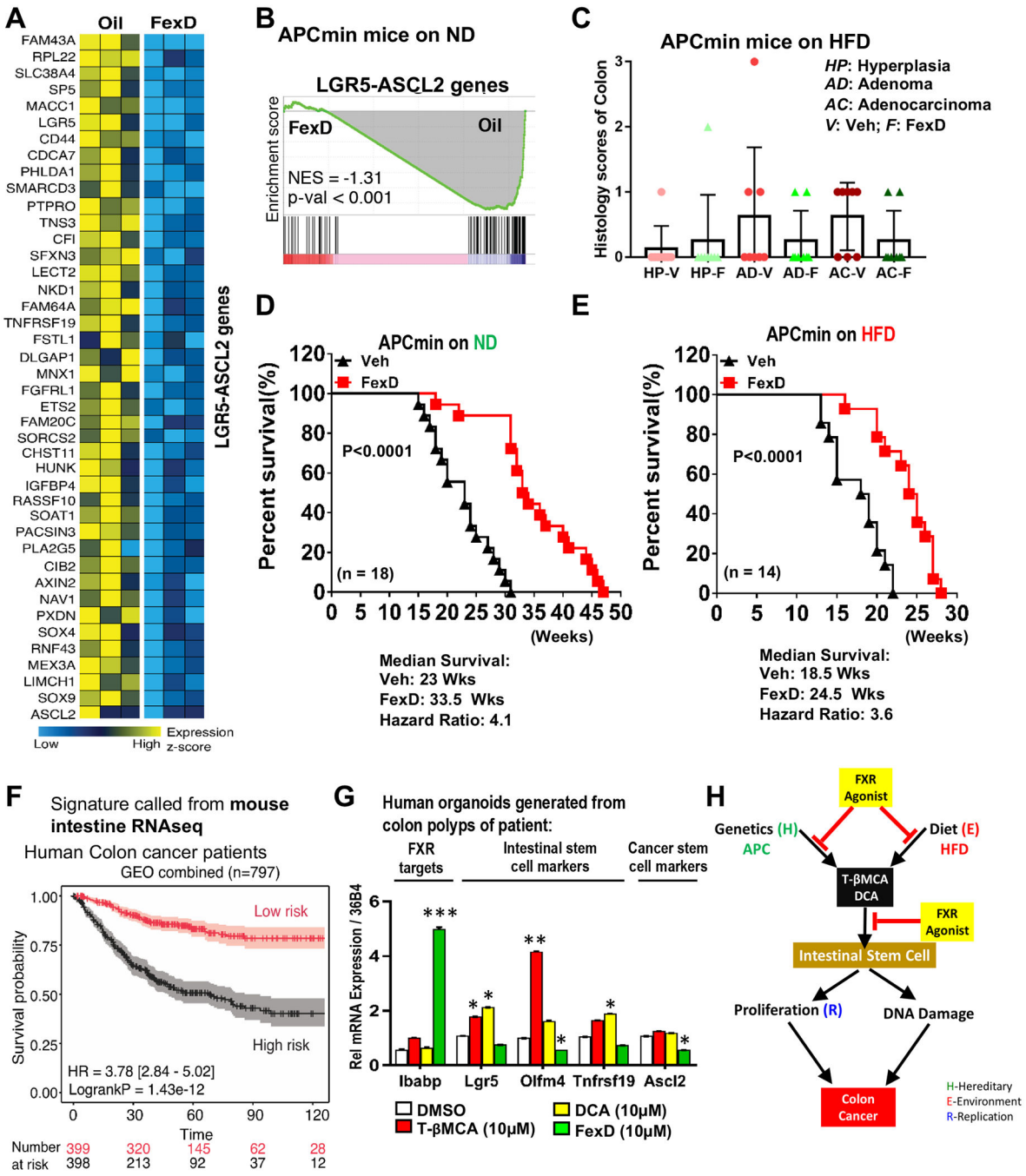

Figure 7. Intestinal FXR agonism improves CRC survival

(**A**) Heatmap of expression changes in stem cell signature (Lgr5-Ascl2) genes in APC$^{min/+}$ mice on ND. Data from 3 representative mice are shown.

(**B**) GSEA of FexD-affected stem cell signature (Lgr5-Ascl2) genes.

(**C**) Histological scores of tumors in APC$^{min/+}$ mice on HFD after FexD or vehicle treatment.

(**D-E**) Survival curves for APC$^{min/+}$ mice on ND (**D**, n=18) and HFD (**E**, n=14) with FexD or vehicle treatment.

(**F**) Parsing of human colon cancer survival curves (797 patients in GEO database) based on a FexD expression signature called from data (**A**).

(**G**) Relative expression of intestinal stem cell genes in organoids generated from polyps collected from human colon cancer patients after treatment with FexD, OCA, T-βMCA and DCA for 1 week.

(**H**) Schematic model depicting the convergence of genetic and dietary risk factors for colon cancer on FXR in intestinal stem cells indicating beneficial effects of FXR agonists.

KEY RESOURCES TABLE

REAGENT or RESOURCE	SOURCE	IDENTIFIER
Antibodies		
Histone H2A.X Antibody	Cell Signaling	Cat#2595 RRID:AB_10694556
Rabbit Anti-Histone H2A.X, phospho (Ser139) Monoclonal Antibody	Cell Signaling	Cat#9718 RRID:AB_2118009
Biological Samples		
Human Organoids generated out of intestinal polyps from Human patients	UCSD	De-identified samples
Chemicals, Peptides, and Recombinant Proteins		
OCA (Obeticholic acid)	Selleck Chemical	Cat#S7660
CDCA (Chenodeoxycholic acid)	Cayman Chemicals	Cat#10011286-5
GW4064	Selleck Chemical	Cat#S782
Fexaramine D	WUXI	Custom order
Tauro-β-muricholic acid (T-pMCA)	Steraloids	Cat# C1899-000
Taurocholic acid (TCA)	Calbiochem	CAS145-42-6
glycolithocholic acid (GLCA)	Steraloids	Cat# C1437-000
deoxycholic acid (DCA)	Steraloids	***Cat# C1070-015***
Hyodeoxycholic Acid (HDCA)	Steraloids	Cat# C0885-000
γ-MCA	Steraloids	Cat# C1850-000
β-MCA	Steraloids	Cat#C1895-000
α-MCA	Steraloids	Cat#C1890-000
ω-MCA	Steraloids	Cat#C1888-000
Cholic-2,2,4,4-d4 acid	C/D/N Isotopes	D-2452
Chenodeoxycholic-2,2,4,4-d4 acid	C/D/N Isotopes	D-2772
Lithocholic-2,2,4,4-d4 acid	C/D/N Isotopes	D-3742
Wnt3a	R&D Systems	Cat #5036-WN-010
5-Fluorouracil (5-FU)	ACROS Organics	Cat #228440010
Critical Commercial Assays		
Total bile acid assay kit	Diazyme laboratories	Cat #DZ042A-K
Fecal occult blood test	Beckman Coulter	Cat# 60151A
Triglyceride kit	Thermo scientific	Cat #TR22421/4780-250
Free fatty acid kit	Bioassay systems	Cat #50-489-265
Bio-Plex Pro Mouse Cytokine 23-plex Assay	Bio-Rad laboratories	M60009RDPD
IL-17 cytokine Elisa kit	Life Technologies	Cat # KMC3021
IL-6 cytokine Elisa kit	Life Technologies	Cat #KMC0061
TNFα cytokine Elisa kit	Life Technologies	Cat #KMC3011
Carcinoembryonic Antigen (CEA) Elisa kit	Lifespan Biosciences	Cat #LS-F5042
Cancer Antigen 19-9 (CA 19-9) Elisa kit	Lifespan Biosciences	Cat #LS-F24309
CellTiter-Glo Luminescent Cell Viability Assay Kit	Promega Corporation	Cat #G7572
CellTiter-Glo Luminescent 3D Cell Viability Assay Kit	Promega Corporation	Cat #G9683
Dual-Luciferase reporter kit	Promega Corporation	Cat #PRE1910

REAGENT or RESOURCE	SOURCE	IDENTIFIER
Cignal TCF/LEF Reporter (luc) Kit	QIAGEN	Cat#CCS-018L
RNeasy Mini Kit	QIAGEN	Cat #74106
RNeasy Micro Kit	QIAGEN	Cat #74004
Arcturus PicoPure RNA isolation kit	Applied Biosystems	Cat #12204-01
Click-iT EdU-A647 flow cytometry kit	Life technologies	Cat #C10424
Click-iT EdU-A647 imaging kit	Life technologies	Cat #C10340
Baseclick EdU *in vivo* kit	Baseclick	BCK488-IV-IM-S
PARP1 (poly ADP-ribose polymerase 1) ELISA Kit	Lifespan Biosciences	Cat #LS-F12266
Bio-Rad iScript Reverse Transcription supermix	Bio-rad	Cat #1708841
Advanced Universal SyBr Green Supermix	Bio-rad	Cat #725271
Western Lightning enhanced chemiluminescence	PerkinElmer Life Sciences	Cat#34095
KaryoMAX Colcemid Solution	GIBCO	Cat#15210-040
Matrigel, growth factor reduced	Corning	Cat #354230
Gentle cell dissociation buffer	Stem Cell	Cat #7174
Intesticult organoid growth medium	Stem Cell	Cat #6005
PBS ($Mg2+/Ca^{2+}$) solution	Corning	Cat # 21-031-CM
FBS	Gemini Bio-products	Cat #900-208
Antibiotic-Antimycotic solution	GIBCO	Cat #15240-062
Deposited Data		
Raw and analyzed RNA-seq data	Illumina High Seq 2500	NCBI's Sequence Read Archive SRP111558
Experimental Models: Cell Lines		
HT29	ATCC	Cat# HTB-38, RRID:CVCL_0320
CACO2	ATCC	Cat# HTB-37, RRID:CVCL_0025
HCT116	ATCC	Cat# CCL-247, RRID:CVCL_0291
HEK293	ATCC	Cat# PTA-4488, RRID:CVCL_0045
Experimental Models: Organisms/Strains		
Mouse: C57BL/6J	The Jackson Laboratory	Cat# JAX:000664, RRID:IMSR_JAX:000664
Mouse: C57BL/6J-ApcMin/J	The Jackson Laboratory	Cat# JAX:002020, RRID:IMSR_JAX:002020
Mouse: B6.129P2-Lgr5tm1 (cre/ERT2)Cle/J	The Jackson Laboratory	Cat# JAX:008875, RRID:IMSR_JAX:008875
Mouse: C57BL/6J-Apctm1Tyj/J	The Jackson Laboratory	JAX:009045, RRID:IMSR_JAX:009045
Mouse: FXR^{flox} mice in C57BL/6J background	Dr. Pierre Chambon (USIAS)	NA
Oligonucleotides		
Primers for RT-qPCR, see Table S5.	IDT	Designed using Primer 3 software
Software and Algorithms		
STAR	Dobin et al., 2013 https://github.com/alexdobin/STAR	N/A
RSEM	Li and Dewey, 2011	N/A
rsem-generate-data-matrix and rsem-run-ebseq commands	Leng et al., 2013	N/A
GSEA	Subramanian et al., 2005	N/A

REAGENT or RESOURCE	SOURCE	IDENTIFIER
Emperor	Caporaso et al., 2010	N/A
SurvExpress	Aguirre-Gamboa et al., 2013	N/A
Homer	http://homer.ucsd.edu/homer/	N/A
CASAVA-1.8.2	https://www.illumina.com/	Illumina
Fiji	https://fiji.sc/	N/A